Modulation of Charge Transfer by *N*-Alkylation to Control Photoluminescence Energy and Quantum Yield

Andrew T. Turley[a], Andrew Danos[b], Antonio Prlj[a], Andrew P. Monkman[b], Basile F. E. Curchod[a], Paul R. McGonigal[a,*], Marc K. Etherington[b,c*]

[a] Department of Chemistry and [b] Department of Physics, Durham University, Lower Mountjoy, Stockton Road, Durham, DH1 3LE, UK. [c] Department of Mathematics, Physics and Electrical Engineering, Northumbria University, Ellison Place, Newcastle upon Tyne, NE1 8ST, UK.

Abstract

Charge transfer in organic fluorophores is a fundamental photophysical process that can be either beneficial, e.g., facilitating thermally activated delayed fluorescence, or detrimental, e.g., mediating emission quenching. *N*-Alkylation is shown to provide straightforward synthetic control of the charge transfer, emission energy and quantum yield of amine chromophores. We demonstrate this concept using quinine as a model. *N*-Alkylation causes changes in its emission that mirror those caused by changes in pH (i.e., protonation). Unlike protonation, however, alkylation of quinine's two N sites is performed in a stepwise manner to give kinetically stable species. This kinetic stability allows us to isolate and characterize an *N*-alkylated analogue of an 'unnatural' protonation state that is quaternized selectively at the less basic site, which is inaccessible using acid. These materials expose (i) the through-space charge-transfer excited state of quinine and (ii) the associated loss pathway, while (iii) developing a simple salt that outperforms quinine sulfate as a quantum yield standard. This *N*-alkylation approach can be applied broadly in the discovery of emissive materials by tuning charge-transfer states.

Introduction

'Your "epipolic" dispersion has given me the clue to a most extensive field of research, which has occupied me during the last year when sunlight permitted' wrote Sir George Stokes to Sir John Herschel on April 6, 1852.[1] This prediction of an extensive field of research has held true through the continued use of spectroscopy to study epipolic dispersion that, also thanks to Stokes, we now know as fluorescence. In recent years, fluorescence spectroscopy has been used to characterize a wide range of different compounds and uncover new functional phenomena such as thermally activated delayed fluorescence (TADF),[2–7] aggregation induced emission[8–10] and room temperature phosphorescence.[11–13]

TADF is of particular interest as it increases the efficiency of organic light-emitting diodes (OLEDs) used in displays and devices. The TADF process is contingent on the formation of charge-transfer (CT) states, i.e., the spatial redistribution of electron density in the excited state. Controlling and tuning CT states is crucial to the development of high efficiency TADF materials.[14] This redistribution can result in reduced overlap between the highest occupied molecular orbital (HOMO) and lowest unoccupied molecular orbital (LUMO).[4,15] CT states also have a significant impact on photochemistry and are commonplace in natural chromophores – for example, they have been invoked in photosynthesis[16–18] and DNA repair[19,20] mechanisms. CT states can contribute to enhancing light emission in organic compounds through mechanisms such as TADF, but their presence is not always desirable. Identification of their behaviour with respect to the electronic energy levels can guide material design.

Here, we utilize quinine (**Qn**) as a model system to demonstrate a strategy for modifying CT states of organic compounds. Recent literature has shown that some of the cinchona

alkaloids display CT and proton transfer, which in turn dictate their photophysical properties.[21,22] These studies have previously been performed using protonation equilibria in aqueous media. Here, we use *N*-alkylation as an alternative in order to permanently modify **Qn**, allowing investigation into the structure–property relationships between lone-pair availability, charge, emission energy and quantum yield. We demonstrate that *N*-alkylation is a versatile method for studying the effects of amine quaternization in aqueous and organic solvent media, not requiring acidic conditions or being subject to equilibria. The kinetic stabilities of the *N*-alkylated salts also make it possible to quaternize structures at positions other than their most basic N site. We identify one N site of **Qn** that can be manipulated to 'turn off' CT state formation and another whose modification tunes emission colour. The compound produced by double *N*-alkylation displays enhanced photoluminescence quantum yields (PLQYs) and solubilities across a range of solvents compared to acidified quinine sulphate (**H_2Qn**·SO_4), which is a common PLQY standard for characterizing blue emitters. Overall, this *N*-alkylation approach represents a simple, robust pathway for tuning the emission and functional properties of **Qn** and other tertiary amines[23–26] to impart functional properties such as improved PLQYs and, potentially, TADF emission.

Results and Discussion

Qn fluoresces blue with a high PLQY in acidified water (55% in 0.1 M aqueous H_2SO_4), but is only weakly emissive at UV wavelengths in basic solution.[27] Recent work has shown that a similar pH-controlled increase in the PLQY of dehydroquinidine, an analogue of **Qn**, is linked to the availability of the quinuclidine lone pair electrons.[21] It has been

proposed that formation of a through-space CT state between the quinuclidine N and the quinoline chromophore leads to quenching of emission. This CT loss pathway is suppressed when the quinuclidine N is protonated, which increases the PLQY. We reasoned that *N*-alkylation of **Qn** could modulate its CT state in a similar manner and that investigation of *N*-alkylated derivatives would allow us to delineate the separate effects of quaternizing each of the two N sites (N1 and N2, Scheme 1) independently of one another, circumventing the intrinsic limitations of using protonation for this task.

We synthesized three salts of methylated **Qn** (Scheme 1). Synthetic procedures and NMR spectroscopic characterisation can be found in Scheme S1 and Figs. S1–S13 in the Supplementary Information. Selective *N*-methylation of the quinuclidine N (N1) is achieved by treating **Qn** with MeI at room temperature,[28] giving **MeQn**$^+$, whereas a reaction temperature of 100 °C leads to **Me$_2$Qn**$^{2+}$ by *N*-methylation of both N1 and the quinoline N (N2).[29,30] This selectivity follows the known basicity trend of N1 and N2.[21,31,32] Methylation at each site gives characteristic changes in ^{1}H NMR chemical shifts (Figs. S14 and S15) and is confirmed by X-ray diffraction (XRD) analysis of single crystals (Scheme 1).‡ By employing an allyl protecting group at N1 (Scheme S1), however, it is also possible to prepare an isomeric form of **MeQn**$^+$ that would be inaccessible using a thermodynamically controlled quaternization approach, such as reversible protonation under acidic conditions. After methylation at N2, the allyl protecting group at N1 is removed to give the kinetically stable ion **iMeQn**$^+$. Each of the cations were isolated with halide counterions before exchanging to BF_4 salts by metathesis with $AgBF_4$ to avoid heavy-nucleus ions with large spin-orbit couplings that might complicate our photophysical investigations by quenching the singlet emission.[33]

The photophysical properties we have measured and modelled for **Qn** and its salts are summarized in Table 1.[34] We first recorded (Fig. 1a) emission spectra of **Qn** dissolved in a series of solvents with a range of polarities. Although the absolute emission intensities from **Qn** in polar organic solvents are low on account of its near-zero PLQY, we could identify distinct emissions from a locally excited (LE) and a CT state.

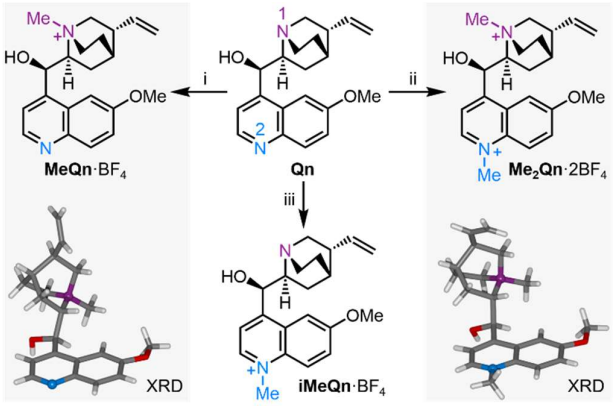

Scheme 1. *N*-Alkylation of **Qn** to *N*-methylquinium tetrafluoroborate, **MeQn**·BF_4, *N*,*N*'-dimethylquinium bis(tetrafluoroborate), **Me_2Qn**·$2BF_4$, and iso-*N*-methylquinium tetrafluoroborate, **iMeQn**·BF_4. XRD structures of **MeQn**·BF_4 and **Me_2Qn**·$2BF_4$ are shown in stick representation with N atoms as balls. Further XRD structures can be found in Figs. S16 and S17 and Table S1. Reagents and conditions: i) a. MeI, rt, 3 d, b. $AgBF_4$, MeCN, 60 °C, 10 min, 74% over 2 steps; ii) MeI, MeCN, 100 °C, 4 h, b. $AgBF_4$, MeOH, rt, 10 min, 79% over 2 steps; iii) a. allyl bromide, CH_2Cl_2, rt, 16 h, b. MeI, MeCN, 100 °C, 3 h, c. barbituric acid, $Pd(PPh_3)_4$ (5 mol%), Me2SO, 40 °C, 16 h, d. diisopropylaminomethyl polystyrene, MeOH, rt, 1 h, e. $AgBF_4$, MeOH, rt, 10 min, 79% over 5 steps.

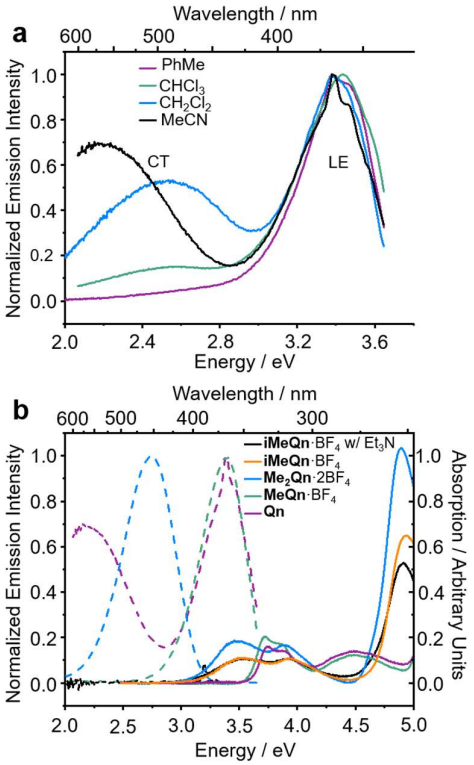

Fig. 1 (a) Steady-state emission spectra of **Qn** dissolved in a series of solvents and excited at 3.75 eV, showing the LE and CT character of its emission. (b) The absorption (solid lines) and emission (dashed lines) spectra of **Qn** (purple), **MeQn**·BF_4 (green), **Me_2Qn**·$2BF_4$ (blue), and **iMeQn**·BF_4 (orange) in MeCN (20 μM). A significant shift in the absorption spectra is associated with the methylation of N2. The emission spectrum of **iMeQn**·BF_4 in MeCN is omitted as partial protonation of N1 by adventitious water affects the spectrum. Instead, the absorption and emission spectra (black) of a MeCN solution of **iMeQn**·BF_4 (20 μM) with Et_3N (10 mM) are displayed to show there is no significant change in absorption with the addition of a base and that there is no emission in the visible region without protonation of N1. The excitation energies (E_{ex}) used were 4.13 eV for **Qn** and **MeQn**·BF_4 or 3.54 eV for **Me_2Qn**·$2BF_4$ and **iMeQn**·BF_4 to allow comparison of PLQYs with known standards (Figs. S18–S26 and Table S2).

A peak in the UV region with emission energy, E_{em}, of 3.4 eV is present in low polarity solvent (PhMe), consistent with emission from an LE state. An additional peak is present in the visible region between 2.2 and 2.6 eV in more polar media. As the polarity is increased when moving from chlorinated solvents to MeCN, the increasing relative intensity of this second peak and its further bathochromic shift are indicative of emission from a CT state.[35–37] The emission spectra are normalized relative to the peak of the LE

(which has reduced intensity in polar solvents) in order to better demonstrate the solvatochromic shift. The intensities of the spectra alone do not illustrate the absolute populations of the states, but the changes in intensity can be rationalised. In apolar solvents there is a higher population of molecules emitting from the LE state, having a high oscillator strength. In polar solvents an important population of molecules is now emitting from the CT state, but the low oscillator strength results in a similar magnitude of emission relative to the LE state. Linear-response time-dependent density functional theory (LR-TDDFT) calculations performed at the ωB97X-D/6-31G* level of theory with state-specific implicit solvation (see supplementary information for full all computational details and benchmarking) support the assignment of these LE and CT bands of **Qn** (Fig. 2). The CT state, in this case, is a result of a through-space charge transfer between the quinuclidine and quinoline system.

Table 1. Photophysical properties of **Qn** and its methylated derivatives.

	Φ[a] / %		E_{em} / eV		Calculated E_{em}[d] / eV		Presence of CT[e]	Red-Shifted Absorption and Emission[f]
Compound	MeCN[b]	H_2O	MeCN[b]	H_2O	LE	CT		
Qn	0	22	3.45 (2.30)	3.20	3.75	1.41	Yes	No
MeQn·BF_4	5	32	3.40	3.24	3.69	-	No	No
Me_2Qn·$2BF_4$	63	70	2.75	2.75	3.00	-	No	Yes
iMeQn·BF_4	0[c]	60	-	2.75	-	1.01	Yes	Yes

[a] PLQYs (Φ) for **Qn** and **MeQn**·BF_4 were measured with respect to a standard of 2-aminopyridine in 0.1 M aqueous H_2SO_4 (Φ = 60%)[38] and those of **Me_2Qn**·$2BF_4$ and **iMeQn**·BF_4 were measured with respect to a standard of **H_2Qn**·SO_4 in 0.1 M aqueous H_2SO_4 (Φ = 55%).[27] [b] Anhydrous MeCN was used throughout the spectroscopic study. [c] Anhydrous MeCN solution with 10 mM Et_3N used to suppress the formation of trace amounts of N1 protonated species resulting from adventitious water [d] Excited-state energies in eV

for protonated (rather than methylated) compounds calculated at the LR-TDDFT/ωB97X-D/6-31G* level of theory with state-specific implicit solvation (MeCN). [e] The presence or lack of an accessible CT state was determined by experimental observation (Fig. 1) and/or theoretical calculation (Tables S5 and S6). [f] Relative to the absorption and emission of **Qn.**

The calculations predict (i) UV emission associated with an electronic transition localized on the quinoline ring system ($\pi \rightarrow \pi^*$) and (ii) a lower energy emission from a CT excited state, which is associated with an electronic transition from a nonbonding orbital located on N1 to an unoccupied π orbital on the quinoline ring ($n \rightarrow \pi^*$). We ascribe **Qn**'s extremely low PLQY (Table 1) to the formation of this through-space CT state. Rapid nonradiative decay from the low-energy CT state, possibly through the low-lying LE triplet state (Fig. S27), serves as a loss pathway that suppresses photoluminescence.[39]

To further confirm this hypothesis and to 'switch on' the UV emission of **Qn**, we investigated the effect of alkylating N1 selectively. Pleasingly, we observed (Fig. 1b) only a single peak in the emission spectrum of **MeQn**·BF_4 at 3.4 eV in MeCN, indicative of emission from the $\pi \rightarrow \pi^*$ LE state of the quinoline ring system. Compared to **Qn**, the peak wavelengths observed in the absorption and emission spectra of **MeQn**·BF_4 are largely unchanged. However, **MeQn**·BF_4 shows no evidence of the lower energy emission from a CT state found for **Qn**. Consequently, **MeQn**·BF_4 emits (Table 1) with an increased PLQY of 5% in MeCN, compared to the near-zero PLQY of neutral **Qn** in MeCN. Quaternization at N1 prevents formation of a CT excited state, removing one of the pathways for rapid nonradiative decay and, as a result, enhancing the PLQY. Similarly, CT state formation is also suppressed for neutral H2O solutions of **Qn**, in which the major species at equilibrium is monoprotonated $\mathbf{HQn}^+$,[31] giving a PLQY of 22%. The PLQY of **MeQn**·BF_4 in H2O solution is 32%.

Methylation of N2 has a markedly different effect on the photoluminescence properties. We first investigated this effect by quaternizing both N1 and N2. The doubly methylated salt **Me$_2$Qn**·2BF$_4$ exhibits (Fig. 1b) significant bathochromic shifts in its absorption and emission energies relative to **Qn** and **MeQn**·BF$_4$. These shifts are reproduced qualitatively by our LR-TDDFT (Table 1) and algebraic diagrammatic construction (ADC(2)) calculations (Tables S3 and S4). Like **MeQn**·BF$_4$, emission from **Me$_2$Qn**·2BF$_4$ (Fig. 2) comes exclusively from the $\pi \rightarrow \pi^*$ LE state. However, the transition is brought into the blue region (2.8 eV) as a result of quaternizing N2.

Extrapolating from our observations based on **MeQn**·BF$_4$ and **Me$_2$Qn**·2BF$_4$, we would expect that selective quaternization of only N2—the less basic N site—would give rise to an ion that retains the CT character of **Qn** on account of the available quinuclidine lone pair electrons (N1), but whose emission and absorption are red-shifted. The LR-TDDFT calculations fit with this hypothesis, predicting (Fig. 2) formation of a new low-energy CT state at lower electronic energy. Moreover, the LR-TDDFT indicates that, upon relaxation of the excited state, the CT state becomes the primary (singlet) 'emissive' state. The selectivity and kinetic stability of the *N*-alkylation approach allows us to test this hypothesis experimentally using **iMeQn**·BF$_4$.

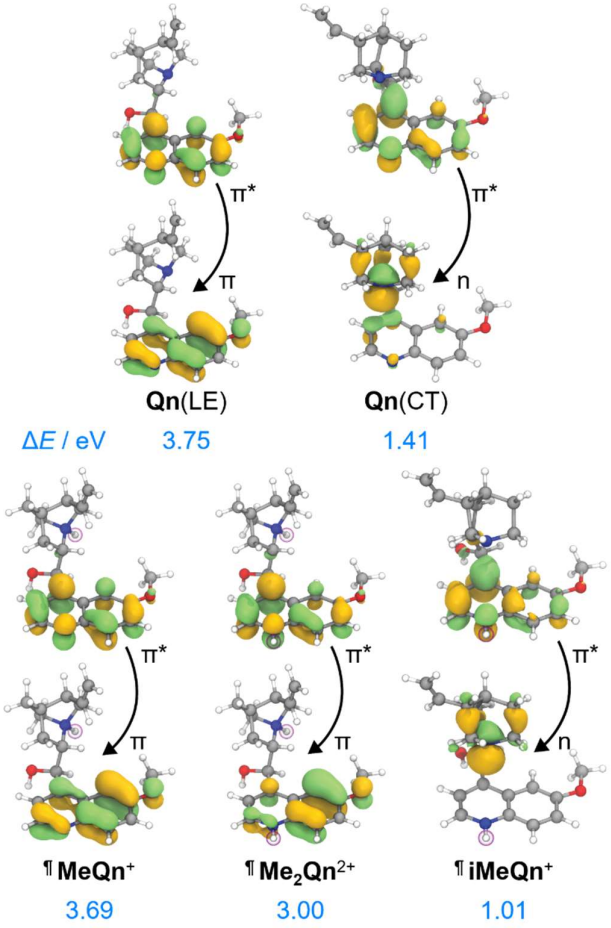

Fig. 2 Natural transition orbitals (NTOs) and energies characterizing the singlet emission of **Qn** from its LE and CT states, as well as **MeQn**$^+$, **iMeQn**$^+$ and **Me$_2$Qn**$^{2+}$, calculated at the LR-TDDFT/ωB97X-D/6-31G* level of theory with state-specific implicit solvation. ¶ Indicates that protonated structures were used as electronically similar (Table S7) models for the methylated salts.

As predicted, the absorption spectrum of **iMeQn**·BF_4 in MeCN matches closely (Fig. 1b) the spectrum of **Me$_2$Qn**·$2BF_4$. Photoluminescence measurements, which were carried out in MeCN with 10 mM triethylamine (Et_3N) to prevent protonation of N1 by adventitious water, are also consistent. Unlike the other methylated derivatives, there is no detectable photoluminescence from **iMeQn**·BF_4. Population of the extremely low-energy CT excited state predicted by calculation appears to lead solely to non-radiative decay. Overall, therefore, selective alkylation of different sites can be used to tune the

photophysical behaviour of **Qn**, modulating independent properties in an orthogonal manner. It is a useful approach to control CT and emission energy. However, the kinetic stabilities and modified solubility profiles of the **Qn** salts also give them advantages over protonated analogues for use as functional materials. For example, while a doubly protonated **Qn** salt, **H_2Qn**·SO_4, is used routinely as a fluorescence standard for relative PLQY measurements in the blue region,[27] its use is limited to acidic aqueous solutions – it is insoluble in common organic solvents and its photoluminescence is quenched in the aggregated state. The physical properties of **Me_2Qn**·$2BF_4$, on the other hand, make it appealing as a more versatile PLQY standard.

Our measurements show that it exhibits an enhanced PLQY of 70% in neutral H_2O compared to the 55% PLQY of **H_2Qn**·SO_4 in 0.1 M aqueous H_2SO_4[27] and, unlike **H_2Qn**·SO_4, it is soluble in organic solvents such as MeCN, EtOH, Me_2CO, CH_2Cl_2, and EtOAc, giving rise to useful PLQYs (Figs. S18–S26 and Table S2) of 63%, 43%, 54%, 48% and 13%, respectively. The variation in PLQY may be a result of modulating ion-pairing between the fluorescent cation and its counterion. Previous investigations of cationic fluorophores have also shown solvent-dependent PLQY and have suggested interactions with the counterion can provide radiationless decay pathways, e.g., through electron transfer and heavy atom effects.[40,41] Overall, however, simple counterion exchange can be used to tune the solubility profile and emission properties. Work is ongoing in our laboratories to optimize these materials as PLQY standards and provide physical insight into the empirical changes in PLQY with solvent.

Conclusions

In summary, we have demonstrated an operationally simple method to tune and elucidate the CT excited states of emissive organic materials by *N*-alkylation. In the present investigation, this approach has allowed us to systematically toggle on and off the presence of a CT excited state, to change the emission colour, and to improve the PLQY of **Qn** – a compound whose photophysical properties were first studied by Herschel and Stokes over 150 years ago.[42–44] This approach can be applied broadly to *N*-heterocycles, which are pervasive structural motifs in many organic chromophores. Resulting insights into their CT excited states will progress our understanding of natural photoactive systems[16–18,45] and improve the performances of emissive[2–7,39] and light-absorbing[46–48] devices. The kinetic stabilities of the *N*-alkylated compounds open up the possibility of quaternizing the chromophores selectively at sites other than their most basic N site, achieving structures that are inaccessible by protonation, while the choice of counterion can serve as a handle to control physical properties.

Conflicts of interest

There are no conflicts to declare.

Acknowledgements

We thank The Royal Society for access to their archives to retrieve the introductory quote, which was transcribed by Melody Bishop. We thank Dr Dmitry Yufit for solving single crystal XRD structures. ATT acknowledges an EPSRC DTG. AD, APM and MKE acknowledge the HyperOLED Horizon 2020 project no. 732013. MKE thanks the Hatfield Trust. This work made use of the facilities of the Hamilton HPC Service of Durham University.

Notes and references

‡ CCDC 1985987 (**MeQn**·BF_4) and 1985988 (**Me_2Qn**·$2BF_4$) contain the supplementary crystallographic data for this paper. These data can be obtained free of charge from The Cambridge Crystallographic Data Centre via www.ccdc.cam.ac.uk/

1 G. G. Stokes, *Sir George Gabriel Stokes to Sir John Frederick William Herschel, 6th April 1852.*, The Royal Society Archive, 1852.

2 H. Uoyama, K. Goushi, K. Shizu, H. Nomura and C. Adachi, *Nature*, 2012, **492**, 234–238.

3 M. K. Etherington, J. Gibson, H. F. Higginbotham, T. J. Penfold and A. P. Monkman, *Nat. Commun.*, 2016, **7**, 13680.

4 F. B. Dias, K. N. Bourdakos, V. Jankus, K. C. Moss, K. T. Kamtekar, V. Bhalla, J. Santos, M. R. Bryce and A. P. Monkman, *Adv. Mater.*, 2013, **25**, 3707–3714.

5 P. Stachelek, J. S. Ward, P. L. dos Santos, A. Danos, M. Colella, N. Haase, S. J. Raynes, A. S. Batsanov, M. R. Bryce and A. P. Monkman, *ACS Appl. Mater. Interfaces*, 2019, **11**, 27125–27133.

6 D. G. Congrave, B. H. Drummond, P. J. Conaghan, H. Francis, S. T. E. Jones, C. P. Grey, N. C. Greenham, D. Credgington and H. Bronstein, *J. Am. Chem. Soc.*, 2019, **141**, 18390–18394.

7 S. Izumi, H. F. Higginbotham, A. Nyga, P. Stachelek, N. Tohnai, P. De Silva, P. Data, Y. Takeda and S. Minakata, *J. Am. Chem. Soc.*, 2020, **142**, 1482–1491.

8 J. Mei, N. L. C. Leung, R. T. K. Kwok, J. W. Y. Lam and B. Z. Tang, *Chem. Rev.*, 2015, **115**, 11718–11940.

9 J. Sturala, M. K. Etherington, A. N. Bismillah, H. F. Higginbotham, W. Trewby, J. A. Aguilar, E. H. C. Bromley, A.-J. Avestro, A. P. Monkman and P. R. McGonigal, *J. Am.*

Chem. Soc., 2017, **139**, 17882–17889.

10 H. Zhang, Z. Zhao, P. R. McGonigal, R. Ye, S. Liu, J. W. Y. Lam, R. T. K. Kwok, W. Z. Yuan, J. Xie, A. L. Rogach and B. Z. Tang, *Mater. Today*, 2020, **32**, 275–292.

11 P. Pander, A. Swist, R. Turczyn, S. Pouget, D. Djurado, A. Lazauskas, R. Pashazadeh, J. V. Grazulevicius, R. Motyka, A. Klimash, P. J. Skabara, P. Data, J. Soloducho and F. B. Dias, *J. Phys. Chem. C*, 2018, **122**, 24958–24966.

12 N. A. Kukhta, R. Huang, A. S. Batsanov, M. R. Bryce and F. B. Dias, *J. Phys. Chem. C*, 2019, **123**, 26536–26546.

13 C. A. M. Salla, G. Farias, M. Rouzières, P. Dechambenoit, F. Durola, H. Bock, B. de Souza and I. H. Bechtold, *Angew. Chemie - Int. Ed.*, 2019, **58**, 6982–6986.

14 R. Huang, N. A. Kukhta, J. S. Ward, A. Danos, A. S. Batsanov, M. R. Bryce and F. B. Dias, *J. Mater. Chem. C*, 2019, **7**, 13224–13234.

15 P. L. dos Santos, M. K. Etherington and A. P. Monkman, *J. Mater. Chem. C*, 2018, **6**, 4842–4853.

16 S. R. Meech, A. J. Hoff and D. A. Wiersma, *Proc. Natl. Acad. Sci. U. S. A.*, 1986, **83**, 9464–9468.

17 V. I. Novoderezhkin, J. P. Dekker and R. van Grondelle, *Biophys. J.*, 2007, **93**, 1293–1311.

18 T. K. Ahn, T. J. Avenson, M. Ballottari, Y.-C. Cheng, K. K. Niyogi, R. Bassi and G. R. Fleming, *Science*, 2008, **320**, 794–797.

19 D. B. Bucher, C. L. Kufner, A. Schlueter, T. Carell and W. Zinth, *J. Am. Chem. Soc.*, 2016, **138**, 186–190.

20 L. Martinez-Fernandez, Y. Zhang, K. de La Harpe, A. A. Beckstead, B. Kohler and R. Improta, *Phys. Chem. Chem. Phys.*, 2016, **18**, 21241–21245.

21 W. Qin, A. Vozza and A. M. Brouwer, *J. Phys. Chem. C*, 2009, **113**, 11790–11795.

22 J. Qian and A. M. Brouwer, *Phys. Chem. Chem. Phys.*, 2010, **12**, 12562–12569.

23 K.-L. Wang, W.-T. Liou, D.-J. Liaw and S.-T. Huang, *Polymer*, 2008, **49**, 1538–1546.

24 J. Zhang, J. Chen, B. Xu, L. Wang, S. Ma, Y. Dong, B. Li, L. Ye and W. Tian, *Chem. Commun.*, 2013, **49**, 3878–3880.

25 S. Achelle, J. Rodríguez-Lopez, C. Katan and F. Robin-Le Guen, *J. Phys. Chem. C*, 2016, **120**, 26986–26995.

26 M. J. Matos, C. D. Navo, T. Hakala, X. Ferhati, A. Guerreiro, D. Hartmann, B. Bernardim, K. L. Saar, I. Compañón, F. Corzana, T. P. J. Knowles, G. Jiménez-Osés and G. J. L. Bernardes, *Angew. Chemie - Int. Ed.*, 2019, **58**, 6640–6644.

27 W. H. Melhuish, *J. Phys. Chem.*, 1961, **65**, 229–235.

28 P. McNeice, F. M. F. Vallana, S. J. Coles, P. N. Horton, P. C. Marr, K. R. Seddon and A. C. Marr, *J. Mol. Liq.*, 2020, **297**, 111773.

29 O. Hesse, *Justus Liebig's Ann. der Chemie*, 1885, **230**, 55–73.

30 A. K. Yadav and A. Singh, *Synlett*, 2000, **8**, 1199–1201.

31 S. G. Schulman, R. M. Threatte, A. C. Capomacchia and W. L. Paul, *J. Pharm. Sci.*, 1974, **63**, 876–880.

32 B. Xiang, K. M. Belyk, R. A. Reamer and N. Yasuda, *Angew. Chemie - Int. Ed.*, 2014, **53**, 8375–8378.

33 J. H. Gutow, *J. Chem. Educ.*, 2005, **82**, 302–305.

34 Emission spectra are reported in eV and are Jacobian corrected to allow meaningful comparisons of Stokes shifts between compounds and emissive states, see: Mooney, J.; Kambhampati, P. *J. Phys. Chem. Lett*. 2013, **4**, 3316

35 B. S. Brunschwig, S. Ehrenson and N. Sutin, *J. Phys. Chem.*, 1987, **91**, 4714–4723.

36 G. Verbeek, S. Depaemelaere, M. Van der Auweraer, F. C. De Schryver, A. Vaes, D. Terrell and S. De Meutter, *Chem. Phys.*, 1993, **176**, 195–213.

37 H. Laguitton-Pasquier, R. Pansu, J.-P. Chauvet, A. Collet, J. Faure and R. Lapouyade, *Chem. Phys.*, 1996, **212**, 437–455.

38 R. Rusakowicz and A. C. Testa, *J. Phys. Chem.*, 1968, **72**, 2680–2681.

39 M. K. Etherington, F. Franchello, J. Gibson, T. Northey, J. Santos, J. S. Ward, H. F. Higginbotham, P. Data, A. Kurowska, P. L. Dos Santos, D. R. Graves, A. S. Batsanov, F. B. Dias, M. R. Bryce, T. J. Penfold and A. P. Monkman, *Nat. Commun.*, 2017, **8**, 14987.

40 I. V. Avilov, A. Y. Panarin and V. S. Chirvony, *Chem. Phys. Lett.*, 2004, **389**, 352–358.

41 V. N. Knyukshto, K. N. Solovyov and G. D. Egorova, *Biospectroscopy*, 1998, **4**, 121–133.

42 J. F. W. Herschel, *Philos. Trans. R. Soc. London*, 1845, **135**, 143–145.

43 G. G. Stokes, *Philos. Trans. R. Soc. London*, 1852, **142**, 463–562.

44 B. Valeur and M. N. Berberan-Santos, *J. Chem. Educ.*, 2011, **88**, 731–738.

45 S. Bai, V. Balevicius, E. Bittner, Y. C. Cheng, M. Chergui, J. Cina, N. Das Neves Rodrigues, A. Datta, J. Dawlaty, A. Dodin, B. Fingerhut, G. Fleming, N. Ginsberg, S. Hammes-Schiffer, V. Huxter, B. Kohler, Y. Lee, G. Leggett, A. Marcus, K. Morenz, J. Ogilvie, A. Olaya-Castro, T. A. A. Oliver, M. Son, Y. Song and V. Stavros, *Faraday Discuss.*, 2019, **216**, 133–161.

46 A. Rao, P. C. Y. Chow, S. Gélinas, C. W. Schlenker, C. Li, H. Yip, A. K.-Y. Jen, D. S. Ginger and R. H. Friend, *Nature*, 2013, **500**, 435–439.

47 M. K. Etherington, J. Wang, P. C. Y. Chow and N. C. Greenham, *Appl. Phys. Lett.*, 2014, **104**, 063304.

48 W. Chang, D. N. Congreve, E. Hontz, M. E. Bahlke, D. P. McMahon, S. Reineke, T. C. Wu, V. Bulović, T. Van Voorhis and M. A. Baldo, *Nat. Commun.*, 2015, **6**, 6415.

Modulation of Charge Transfer by *N*-Alkylation to Control Fluorescence Energy and Quantum Yield

Andrew T. Turley[a], Andrew Danos[b], Antonio Prlj[a], Andrew P. Monkman[b], Basile F. E. Curchod[a], Paul R. McGonigal[a,*], Marc K. Etherington[b,c*]

[a] Department of Chemistry and [b] Department of Physics, Durham University, Lower Mountjoy, Stockton Road, Durham, DH1 3LE, UK. [c] Department of Mathematics, Physics and Electrical Engineering, Northumbria University, Ellison Place, Newcastle upon Tyne, NE1 8ST, UK.

Table of Contents

1. General Methods S1
2. Synthetic Procedures S3
3. ^{1}H, ^{13}C and ^{19}F NMR Spectroscopic Characterisation of Synthesised Compounds S8
4. X-Ray Crystallographic Analysis S23
    4.1. **MeQn**·BF_4 S23
    4.2. **Me_2Qn**·$2BF_4$ S24
5. Photoluminescence Quantum Yield Measurements S26
6. Phosphorescence of **Qn** in a Zeonex Film S36
7. Theoretical Study S37
8. References S43

Supporting Information

1. General Methods

Materials: All reagents were purchased from commercial suppliers (Sigma-Aldrich, Acros Organics, or Alfa Aesar) and used without further purification.

Instrumentation and Analytical Techniques: Analytical thin-layer chromatography (TLC) was performed on neutral aluminium-sheet silica gel plates and visualised under UV irradiation (254 nm). Nuclear magnetic resonance (NMR) spectra were recorded using a Bruker Advance (III)-400 (^{1}H 400.130 MHz and ^{13}C 100.613 MHz), Varian Inova-500 (^{1}H 500.130 MHz and ^{13}C 125.758 MHz), Varian VNMRS-600 (^{1}H 600.130 MHz and ^{13}C 150.903 MHz) or a Varian VNMRS-700 (^{1}H 700.130 MHz and ^{13}C 176.048 MHz) spectrometers, at a constant temperature of 298 K unless otherwise stated. Chemical shifts (δ) are reported in parts per million (ppm) relative to the signals corresponding to residual non-deuterated solvents [DMSO-*d6*: δ = 2.50 or 39.52. CD_3OD: δ = 3.31 or 49.00]. Coupling constants (J) are reported in Hertz (Hz). ^{13}C NMR Experiments were proton-decoupled, whereas ^{19}F NMR experiments are coupled and referenced to an internal standard, hexafluorobenzene (HFB, δ = 164.99 ppm). Assignments of ^{1}H and ^{13}C NMR signals were accomplished by two-dimensional NMR spectroscopy (COSY, NOESY, HSQC, HMBC). NMR spectra were processed using MestReNova version 12. Data are reported as follows: chemical shift; multiplicity; coupling constants; integral and assignment. High-resolution electrospray (HR-ESI) mass spectra were measured using a Waters LCT Premier XE high resolution, accurate mass UPLC ES MS. Melting points were recorded using a Gallenkamp (Sanyo) apparatus and are uncorrected. UV-Vis-NIR absorbance spectra of solution samples were recorded using an Agilent Technologies Cary Series UV-vis-NIR spectrophotometer at room temperature. Steady-state photoluminescence of films and solutions were measured using a Jobin Yvon Fluoromax or Fluorolog with machine-specific calibration curves. The photoluminescence quantum yields (PLQYs) of the compounds were

measured using the relative method[1] and comparing to known standards of quinine sulfate[2] and 2-aminopyridine[3] in aqueous 0.1 M H_2SO_4. The absorption spectra and photoluminescence spectra for the PLQYs were measured on a Shimadzu UV-3600 UV-VIS-NIR spectrophotometer and a Jobin Yvon Fluoromax or Fluorolog. The low temperature phosphorescence spectrum of **Qn** in a zeonex film was acquired by placing the sample in a Janis Research VNF-100 cryostat, used in conjunction with a Lakeshore 332 temperature controller, and exciting the sample with 337nm light from an N_2 laser (LTBMNL 100, Lasertechnik Berlin) at 10 Hz. Sample emission was the directed onto a spectrograph and gated iCCD camera (Stanford Computer Optics). The X-ray single crystal data were collected at a temperature of 120.0(2) K using λCuKα radiation (λ = 1.54178 Å) on a Bruker D8Venture (Photon100 CMOS detector, IμS-microsource, focusing mirrors) diffractometer equipped with a Cryostream (Oxford Cryosystems) open-flow nitrogen cryostat. Both structures were solved by direct method and refined by full-matrix least squares on F^2 for all data using Olex2[4] and SHELXTL[5] software. All non-disordered non-hydrogen atoms were refined anisotropically, closely located disordered atoms in structure **MeQn**·BF_4 were refined isotropically. The disordered atoms were refined with fixed site occupation factors 0.6 and 0.4. Hydrogen atoms in structure **Me$_2$Qn**·2BF_4 and in OH-groups of structure **MeQn**·BF_4 were refined isotropically, the remaining hydrogen atoms in structure **MeQn**·BF_4 were placed in the calculated positions and refined in riding mode. The absolute configuration of studied compounds was determined from anomalous scattering by calculating the Flack[6] (*x*) and Hooft[7] (*y*) parameters which should equal 0 for the correct absolute structure and 1 for the inverted model. Crystal data and parameters of refinement are listed in Table S1. Crystallographic data for the structure have been deposited with the Cambridge Crystallographic Data Centre as supplementary publication CCDC-1985987-1985988.

2. Synthetic Procedures

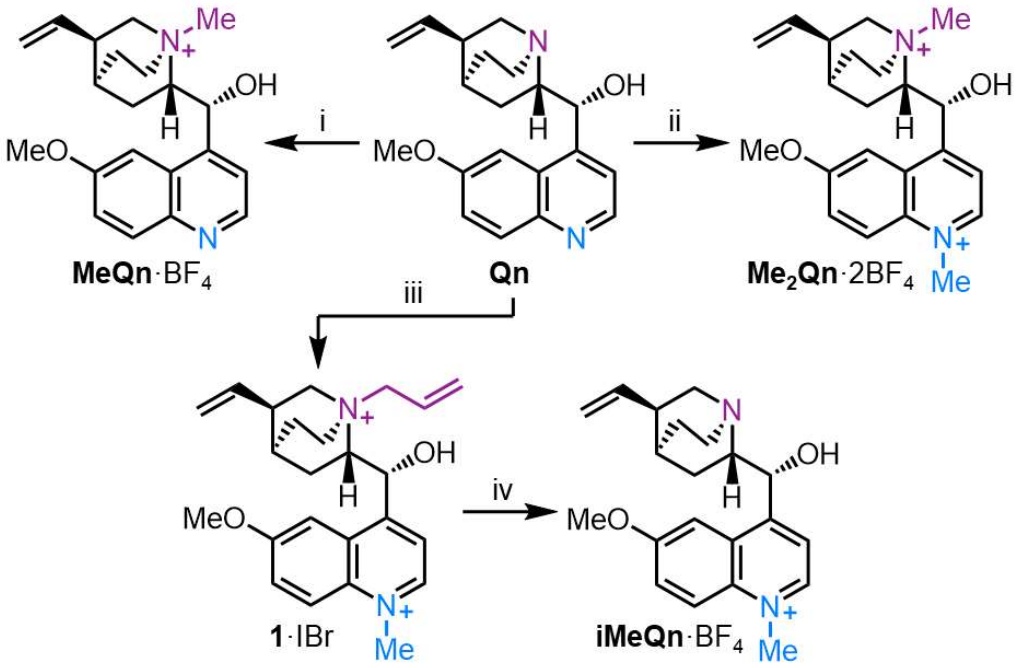

Scheme S1 Synthetic routes to **MeQn**·BF_4, **Me_2Qn**·BF_4 and **iMeQn**·BF_4. Reagents and conditions: (i) a) MeI / rt / 3 d, b) $AgBF_4$ / MeCN / 60 °C / 10 min; (ii) a) MeI / MeCN / 100 °C / 4 h, b) $AgBF_4$ / MeOH / rt / 10 min, (iii) a) Allyl bromide / CH_2Cl_2 / rt / 16 h, b) MeI / MeCN / 100 °C / 3 h; (iv) (a) Barbituric acid / $Pd(PPh_3)_4$ (5 mol%) / Me_2SO / 40 °C / 16 h, (b) Diisopropylaminomethyl polystyrene / MeOH / rt / 1h, c) $AgBF_4$ / MeOH / rt / 10 min.

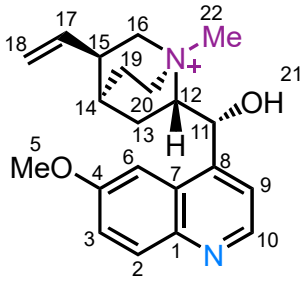

MeQn·BF_4: Quinine (500 mg, 1.54 mmol) was added to an oven-dried microwave vial and sealed. MeI (5 mL) was added and the mixture was sonicated at rt for 20 min. The reaction mixture was stirred for 3 days at rt. The mixture was filtered to isolate the precipitate, washing with CH_2Cl_2 (2 × 5 mL) and drying the precipitate under high vacuum. The resulting solid was recrystallized from MeCN to yield the iodide salt of title compound, **MeQn**·I, as a crystalline solid (618 mg, 1.23 mmol, 80 %). **MeQn**·I (106 mg, 0.227 mmol) was dissolved in MeCN (8 mL) and heated to 60 °C. A solution of $AgBF_4$ (44.0 mg, 0.227 mmol) in MeCN (1 mL) was added dropwise and allowed to stir at 60 °C

for 10 min. The resulting mixture was filtered and the filtrate was evaporated to dryness to give the title compound as a colourless solid (87 mg, 0.20 mmol, 93%). **M.P.** 185 – 187 °C. **^{1}H NMR** (700 MHz, DMSO-d_6) δ 8.79 (d, J = 4.5 Hz, 1H, H_{10}), 8.00 (d, J = 9.2 Hz, 1H, H_2), 7.70 (d, J = 4.9 Hz, 1H, H_9), 7.48 (dd, J = 9.2, 2.7 Hz, 1H, H_3), 7.21 (d, J = 2.7 Hz, 1H, H_6), 6.54 (d, J = 2.7 Hz, 1H, H_{21}), 6.21 (d, J = 3.2 Hz, 1H, H_{11}), 5.75 (ddd, J = 17.3, 10.5, 6.8 Hz, 1H, H_{17}), 5.13 – 5.01 (m, 2H, H_{18}), 4.07 (m, 1H, H_{20}), 4.00 (s, 3H, H_5), 3.74 – 3.60 (m, 3H, H_{16+12}), 3.45 – 3.35 (m, 4H, H_{20+22}), 2.85 – 2.76 (m, 1H, H_{15}), 2.20 – 2.10 (m, 2H, H_{13+19}), 2.06 – 2.01 (m, 1H, H_{14}), 1.97 – 1.87 (m, 1H, H_{19}), 1.38 – 1.31 (m, 1H, H_{13}). **^{13}C NMR** (176 MHz, DMSO-d_6) δ 157.4 (C_4), 147.4 (C_{10}), 143.8 (C_8), 143.6 (C_1), 137.9 (C_{17}), 131.5 (C_2), 125.1 (C_7), 121.5 (C_3), 119.9 (C_9), 116.5 (C_{18}), 101.6 (C_6), 66.78 (C_{12}), 63.9 (C_{11} + C_{16}), 55.48 (C_5), 54.2 (C_{20}), 48.7 (C_{22}), 37.6 (C_{15}), 25.9 (C_{14}), 24.6 (C_{19}), 19.3 (C_{13}). **^{19}F NMR** (376 MHz, CD_3OD) δ -150.48 (m, ^{10}B), -150.54 (m, ^{11}B). **HR-ESI-MS** m/z = 339.2088 $[M\text{-}BF_4]^+$ (calculated for $C_{21}H_{27}N_2O_2$ = 339.2073).

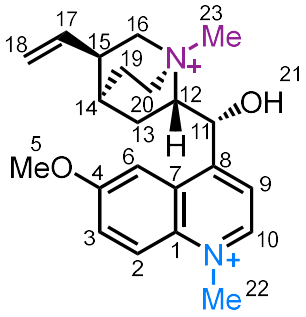

Me$_2$Qn·2BF_4: Quinine (2.00 g, 6.17 mmol) was added to an oven-dried microwave vial and sealed. MeCN (18 mL) was added and stirred at rt before adding MeI (1.92 mL, 30.8 mmol). The resulting mixture was heated at 100 °C for 4 h then allowed to cool to rt and further cooled to 5 °C in a fridge to allow the product to crystallise. The supernatant was decanted and the resulting crystals were isolated and dried under high vacuum to give the diiodide salt of the title compound (2.98 g, 4.9 mmol, 79%). **Me$_2$Qn**·2I (200 mg, 0.329 mmol) was dissolved in MeOH (5 mL) and a solution of $AgBF_4$ (128 mg, 0.658 mmol) in MeOH (5 mL) was added dropwise and stirred at rt for 10 min. The reaction mixture was filtered and the filtrate was evaporated to dryness to yield the

title compound as a colourless solid (135 mg, 0.329 mmol, quantitative). **M.P.** 195 – 197 °C. **^{1}H NMR** (600 MHz, DMSO-d_6) δ 9.32 (d, J = 6.1 Hz, 1H, H_{10}), 8.51 (d, J = 9.7 Hz, 1H, H_2), 8.28 (d, J = 6.0 Hz, 1H, H_9), 7.99 (dd, J = 9.7, 2.6 Hz, 1H, H_3), 7.54 (d, J = 2.7 Hz, 1H, H_6), 7.16 – 7.05 (m, 1H, H_{21}), 6.53 – 6.46 (m, 1H, H_{11}), 5.70 (ddd, J = 17.3, 10.5, 6.9 Hz, 1H, H_{17}), 5.13 – 5.03 (m, 2H, H_{18}), 4.62 (s, 3H, H_{22}), 4.14 (m, 4H, H_{5+20}), 3.77 – 3.61 (m, 3H, H_{12+16}), 3.48 – 3.38 (m, 4H, H_{20+23}), 2.87 – 2.79 (m, 1H, H_{15}), 2.10 (m, 3H, H_{13+19}), 2.00 – 1.92 (m, 1H, H_{14}), 1.36 (m, 1H, H_{13}). **^{13}C NMR** (151 MHz, DMSO-d_6) δ 159.3 (C_4), 154.9 (C_1), 146.3 (C_{10}), 137.9 (C_{17}), 133.6 (C_8), 127.1 (C_7), 126.6 (C_3), 121.8 (C_2), 121.1 (C_9), 116.6 (C_{18}), 103.9 (C_6), 66.2 (C_{12}), 64.5 (C_{11}), 64.2 (C_{16}), 56.3 (C_5), 54.4 (C_{20}), 48.8 (C_{23}), 45.6 (C_{22}), 37.4 (C_{15}), 25.8 (C_{14}), 24.6 (C_{19}), 19.4 (C_{13}). **^{19}F NMR** (376 MHz, CD_3OD) δ -150.49 (m, ^{10}B), -150.54 (m, ^{11}B). **HR-ESI MS** m/z = 440.2379 $[M\text{-}BF_4]^+$ (calculated for $C_{22}H_{30}N_2O_2{}^{10}BF_4$ = 440.2373).

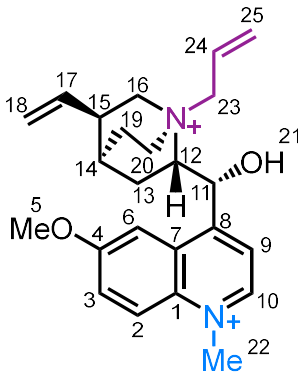

1·IBr: Quinine (500 mg, 1.54 mmol) was placed into an oven-dried round-bottomed flask. CH_2Cl_2 (2.5 mL) was added and stirred at rt before adding allyl bromide (0.13 mL, 1.54 mmol). The resulting solution was stirred at rt for 16 h. Once the reaction was complete, the volatiles were removed under vacuum. The resulting solid was dissolved in MeCN (2.5 mL) and MeI (0.13 mL, 2.09 mmol) was added dropwise and the mixture was heated to 100 °C for 3 h. The mixture was allowed to cool to rt and further cooled to 5 °C in a fridge to allow the product to precipitate. The orange precipitate was isolated by filtration and washed with CH_2Cl_2 (2 × 5 mL), then dried under high vacuum to give the title compound as an orange solid (710 mg, 1.25 mmol, 81%). **M.P**. 203 – 205 °C. **^{1}H NMR** (400 MHz, DMSO-d_6) δ 9.32 (d, J = 6.1 Hz, 1H, H_{10}), 8.50 (d, J = 9.7 Hz, 1H, H_2), 8.25 (d, J = 6.0 Hz, 1H, H_9), 8.00 (dd, J = 9.7, 2.7 Hz, 1H, H_3), 7.54 (d, J = 2.7 Hz, 1H, H_6), 7.10 (d, J = 4.1 Hz, 1H, H_{21}), 6.55 (m, 1H, H_{11}), 6.26 (m, 1H, H_{24}), 5.81 – 5.59 (m, 3H, H_{17+23}), 5.09 –

4.97 (m, 2H, H_{18}), 4.58 (s, 3H, H_{22}), 4.54 (m, 1H, H_{25}) 4.29 (m, 1H, H_{25}), 4.12 (s, 3H, H_5), 4.05 – 3.96 (m, 1H, H_{20}), 3.76 – 3.65 (m, 2H, H_{12+16}), 3.57 – 3.39 (m, 2H, H_{16+20}), 2.79 (m, 1H, H_{15}), 2.13 – 1.96 (m, 4H, $H_{13+14+19}$), 1.32 (m, 1H, H_{13}). **^{13}C NMR** (101 MHz, DMSO-*d*$_6$) δ 159.4 (C_4), 154.9 (C_1), 146.4 (C_{10}), 138.1 (C_{17}), 133.7 (C_8), 127.5 (C_{23}), 127.3 (C_7), 126.6 (C_3), 126.2 (C_{24}), 121.9 (C_2), 121.5 (C_9), 116.7 (C_{18}), 104.4 (C_6), 65.9 (C_{12}), 64.6 (C_{11}), 62.5 (C_{25}), 60.3 (C_{16}), 56.5 (C_5), 52.2 (C_{20}), 45.7 (C_{22}), 37.3 (C_{15}), 26.1 (C_{14}), 24.5 (C_{19}), 20.4 (C_{13}). **HR-ESI-MS** *m/z* = 507.1505 $[M\text{-}Br]^+$ (calculated for $C_{24}H_{32}N_2O_2I$ = 507.1508).

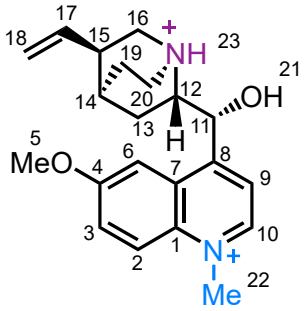

H-iMeQn·2Cl**:** **1**·IBr (80 mg, 0.14 mmol) was dissolved in Me_2SO (1 mL) then $Pd(PPh_3)_4$ (8 mg, 6.92 µM, 5 mol%) and barbituric acid (52 mg, 0.4 mmol) were added to the reaction mixture and stirred overnight at 40 °C. A 1 M aqueous solution of HCl (1 mL) was added and stirred for 5 min. The mixture was then purified by reverse phase column chromatography (Teledyne Isco CombiFlash Rf+ system, 40 g C18-capped SiO_2, 0.05 M HCl(aq) / MeOH, 0 – 100% elution). After evaporation, the product was isolated as a yellow film (57 mg, 0.14 mmol, quantitative). **^{1}H NMR** (400 MHz, DMSO-*d*$_6$) δ 9.14 (d, *J* = 6.1 Hz, 1H, H_{10}), 8.45 (d, *J* = 9.8 Hz, 1H, H_2), 8.28 (d, *J* = 6.1 Hz, 1H, H_9), 7.88 (m, 2H, H_{3+6}), 6.51 (s, 1H, H_{11}), 5.75 (ddd, *J* = 17.4, 10.4, 7.2 Hz, 1H, H_{17}), 5.10 – 5.00 (m, 2H, H_{18}), 4.63 (s, 3H, H_{22}), 4.27 – 4.19 (m, 1H, H_{20}), 4.16 (s, 3H, H_5), 3.67 (m, 1H, H_{12}), 3.60 (m, 1H, H_{16}), 3.31 (m, 1H, H_{16}), 3.24 (m, 1H, H_{20}) 2.81 (m, 1H, H_{15}), 2.19 (m, 2H, H_{13+19}), 2.09 (m, 1H, H_{14}), 1.98 (m, 1H, H_{19}), 1.57 (m, 1H, H_{13}). **^{13}C NMR** (101 MHz, DMSO-*d*$_6$) δ 162.4 (C_4), 158.0 (C_1), 147.1 (C_{10}), 139.2 (C_{17}), 135.9 (C_8), 129.8 (C_7), 129.4 (C_3), 122.4 (C_2), 121.6 (C_9), 117.3 (C_{18}), 104.5 (C_6), 68.1 (C_{11}), 60.9

(C_{12}), 58.6 (C_5), 55.5 (C_{16}), 46.5 (C_{23}), 45.3 (C_{20}), 38.5 (C_{15}), 28.4 (C_{14}), 25.1 (C_{19}), 19.2 (C_{13}). **HR-ESI-MS** *m/z* = 409.1472 $[M\text{-}H]^+$ (calculated for $C_{21}H_{27}N_2O_2Cl_2$ = 409.1449).

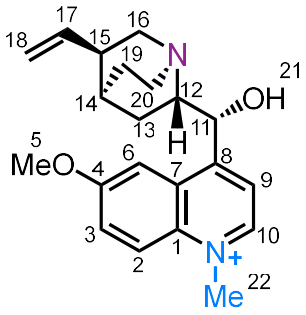

iMeQn·BF_4: **H-iMeQn**·2Cl (64 mg, 0.16 mmol) was dissolved in MeOH (10 mL) and diisopropylaminomethyl polystyrene (467 mg, 1.4 mmol, 200–400 mesh particle size, extent of labelling: ~3 mmol/g base loading, matrix crosslinked with 2% divinylbenzene) was added. The reaction mixture was stirred for 1 h at rt before being filtered. The filtrate was evaporated to dryness and washed with hexanes (5 × 10 mL) to extract any solubilised polymer. The residual solid was dried under high vacuum to yield **iMeQn**·Cl (45 mg, 0.12 mmol, 86%). The chloride salt was dissolved in MeOH (3 mL) and a solution of $AgBF_4$ (23 mg, 0.12 mmol) in MeOH (2 mL) was added dropwise then stirred for 10 min at rt. The reaction mixture was filtered and the filtrate was evaporated to dryness to yield the title compound as an off white solid (51 mg, 0.12 mmol, quantitative). **M.P.** 204 – 206 °C. **^{1}H NMR** (400 MHz, CD_3OD) δ 9.14 (d, *J* = 6.1 Hz, 1H, H_{10}), 8.48 (d, *J* = 9.7 Hz, 1H, H_2), 8.27 (d, *J* = 6.1 Hz, 1H, H_9), 7.92 (d, *J* = 9.7, 2.4 Hz, 1H, H_3), 7.87 (m, 1H, H_6), 6.24 (s, 1H, H_{11}), 5.79 (ddd, *J* = 17.4, 10.4, 7.2 Hz, 1H, H_{17}), 5.10 – 5.01 (m, 2H, H_{18}), 4.65 (s, 3H, H_{22}), 4.16 (s, 3H, H_5), 4.06 (m, 1H, H_{20}), 3.52 (m, 1H, H_{12}), 3.48 (m, 1H, H_{16}), 3.13 (m, 2H, H_{16+20}), 2.70 (m, 1H, H_{15}), 2.14 (m, 3H, H_{13+19}), 2.04 (m, 1H, H_{14}) 1.87 (m, 1H, H_{19}), 1.61 (m, 1H, H_{13}). **^{13}C NMR** (101 MHz, CD_3OD) δ 162.1 (C_4), 147.2 (C_{10}), 140.1 (C_{17}), 135.9 (C_8), 129.9 (C_7), 129.0 (C_3), 122.4 (C_2), 121.5 (C_9), 116.7 (C_{18}), 104.5 (C_6), 69.4 (C_{11}), 61.2 (C_{12}), 57.7 (C_5), 56.2 (C_{16}), 46.4 (C_{22}), 45.2 (C_{20}), 39.2 (C_{15}), 28.5 (C_{14}), 25.9 (C_{19}), 20.2 (C_{13}). **^{19}F NMR** (376 MHz, CD_3OD) δ -153.71 (m, ^{10}B), -153.76 (m, ^{11}B). **HR-ESI-MS** *m/z* = 339.2087 $[M\text{-}BF_4]^+$ (calculated for $C_{21}H_{27}N_2O_2$ = 339.2037).

3.1 ^{1}H, ^{13}C and ^{19}F NMR Spectroscopic Characterisation of Synthesised Compounds

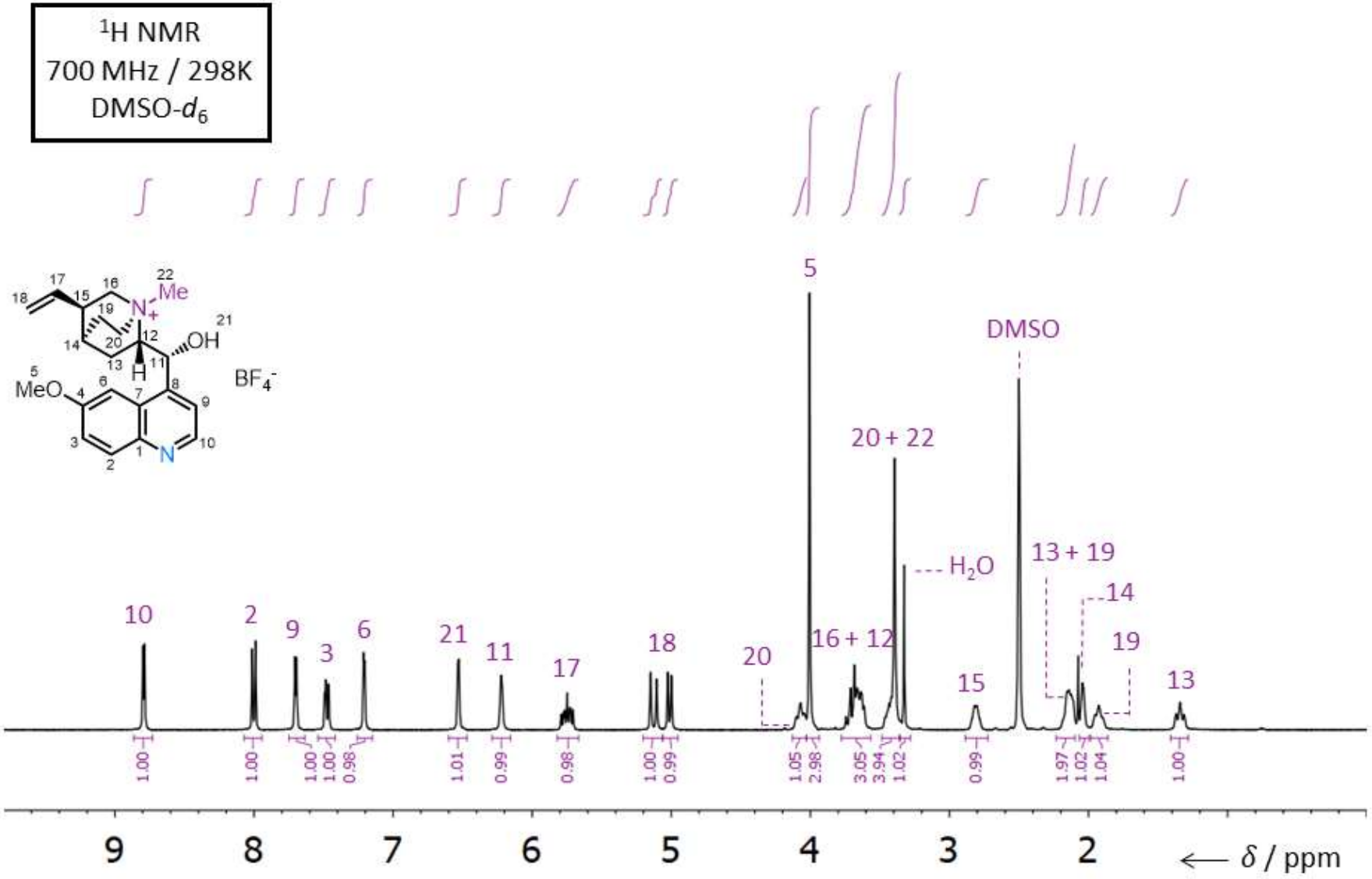

Fig. S1 ^{1}H NMR Spectrum of **MeQn**·BF_4.

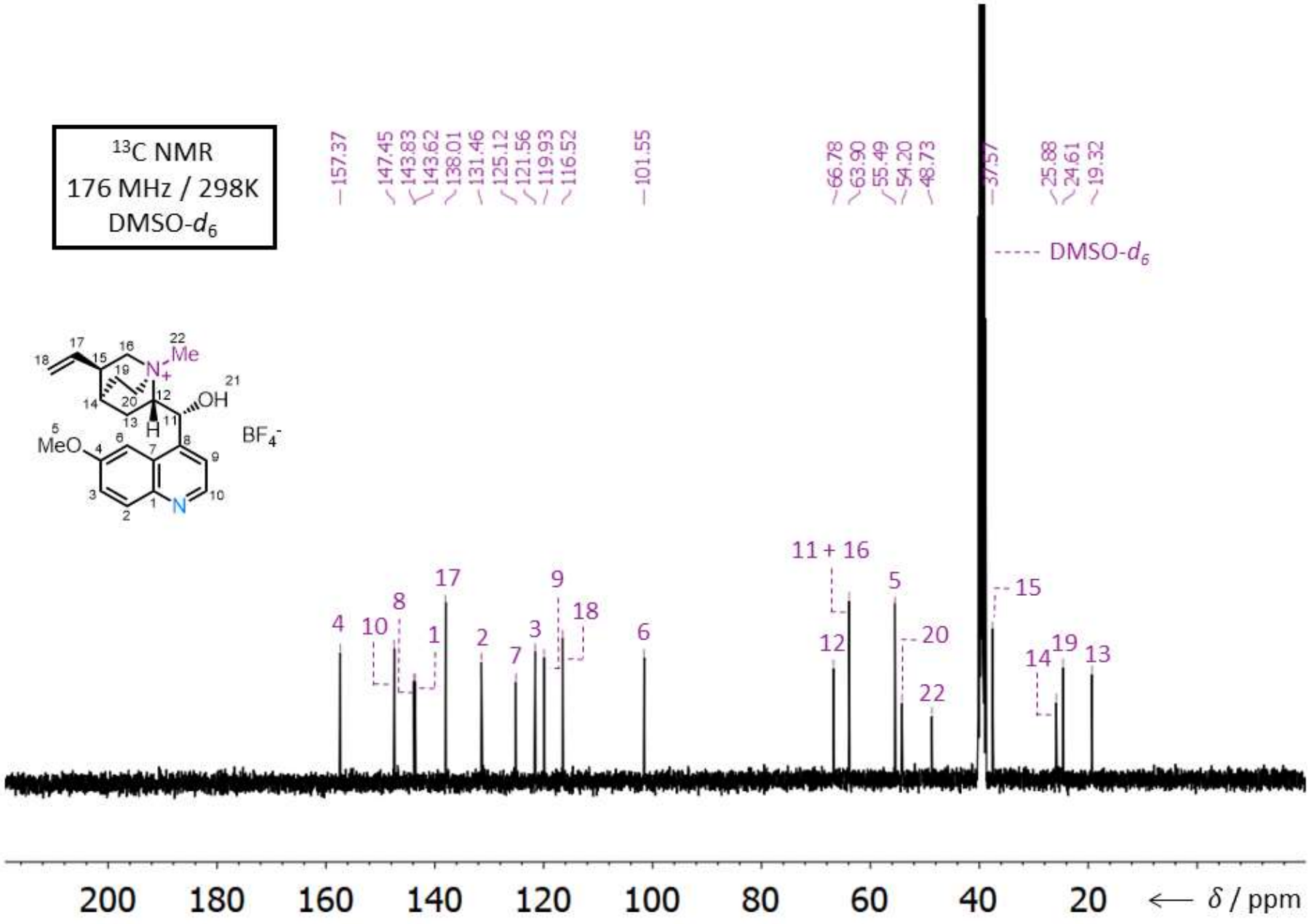

Fig. S2 ^{13}C NMR Spectrum of **MeQn**·BF_4.

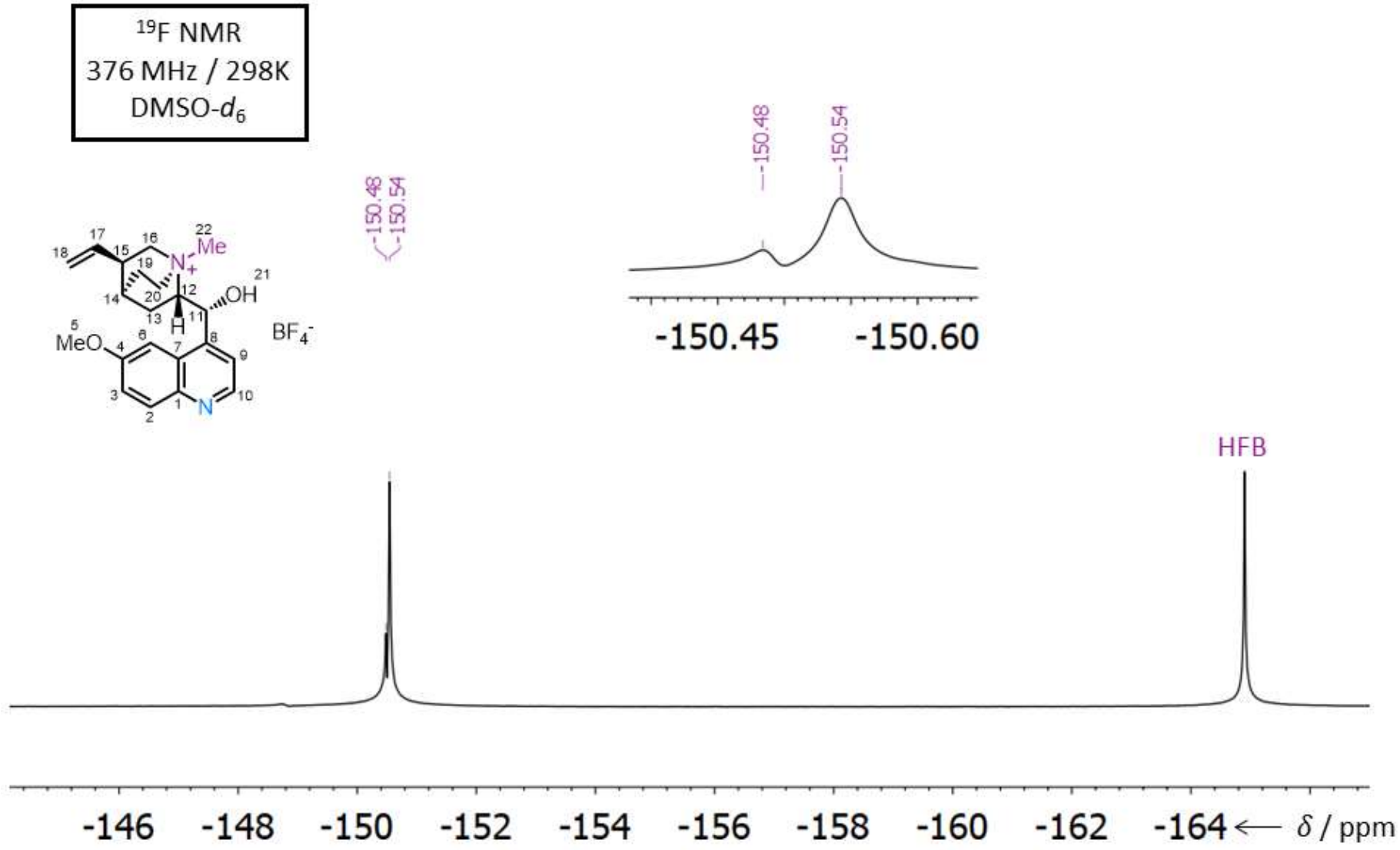

Fig. S3 ^{19}F NMR Spectrum of **MeQn**·BF_4.

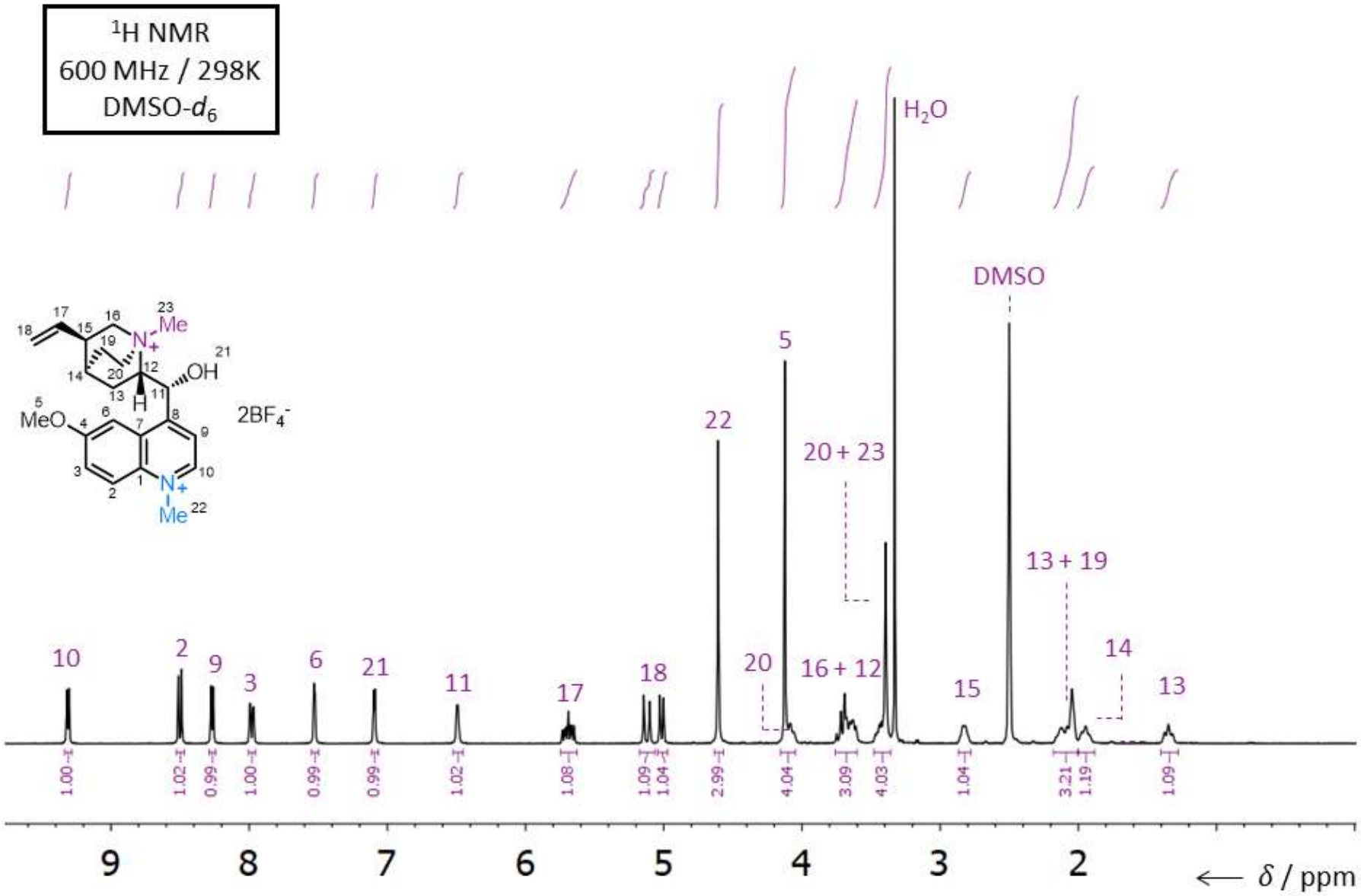

Fig. S4 ^{1}H NMR Spectrum of **Me$_2$Qn**·BF$_4$.

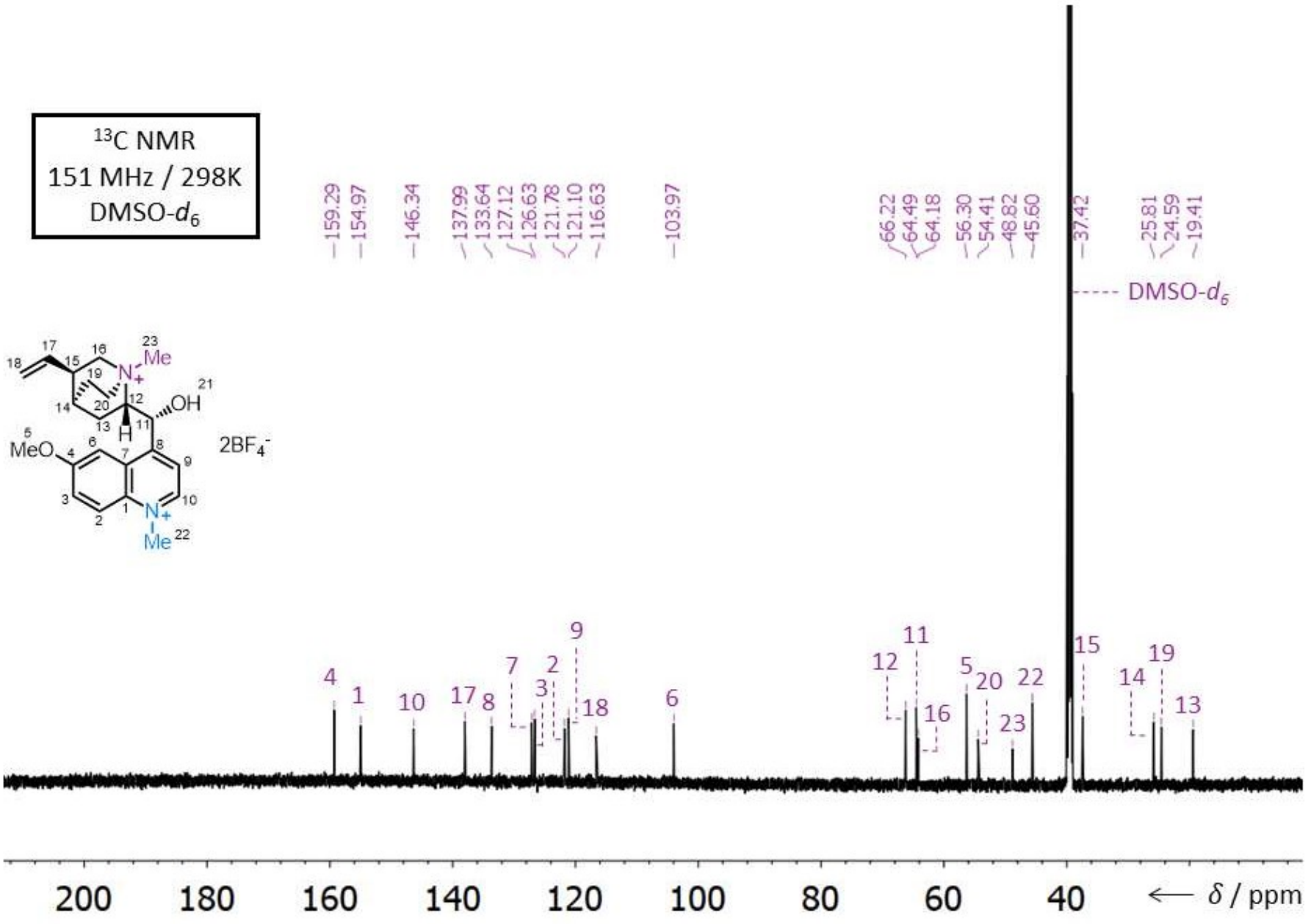

Fig. S5 ^{13}C NMR Spectrum of **Me$_2$Qn**·BF$_4$.

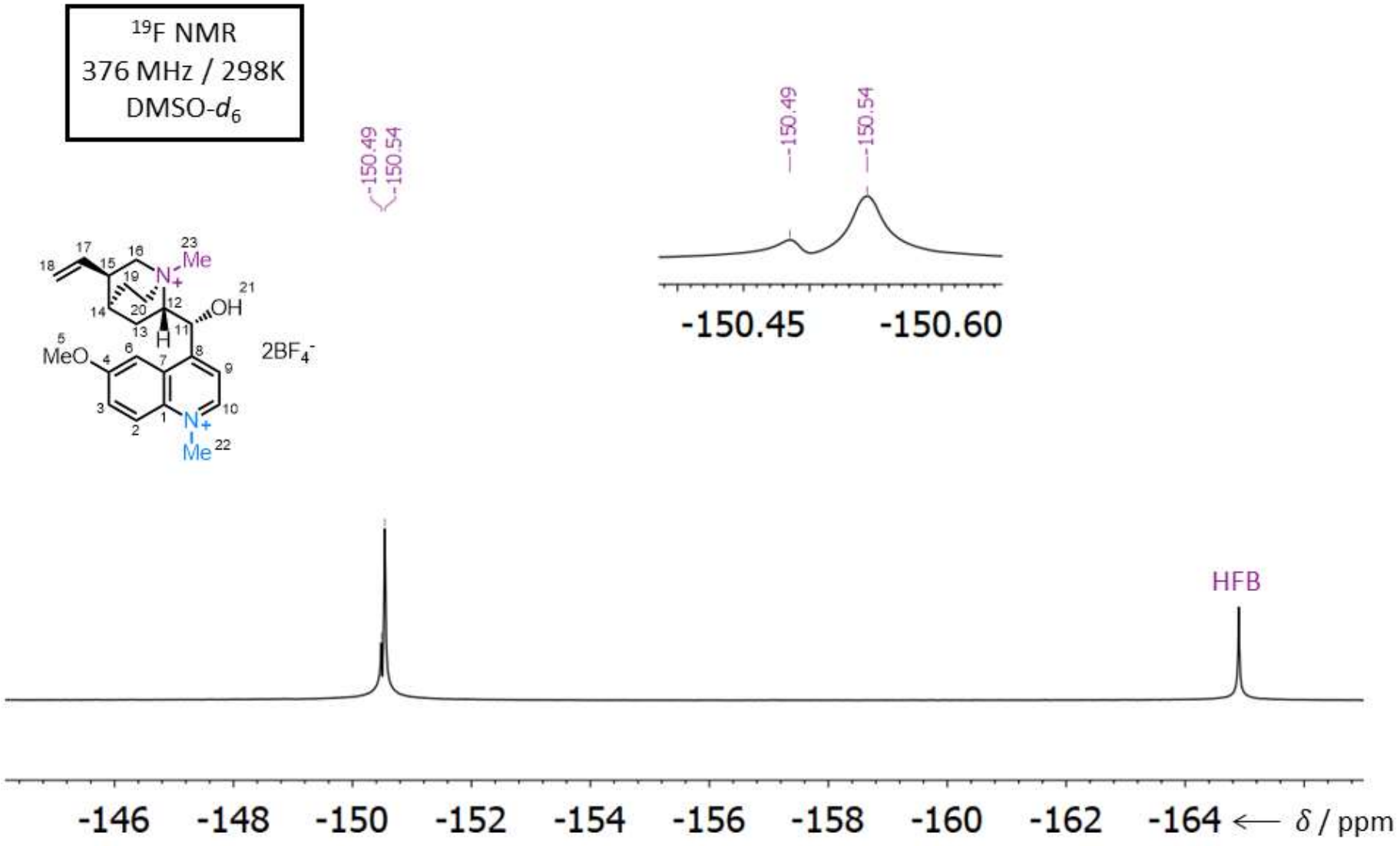

Fig. S6 ^{19}F NMR Spectrum of **Me$_2$Qn**·BF_4.

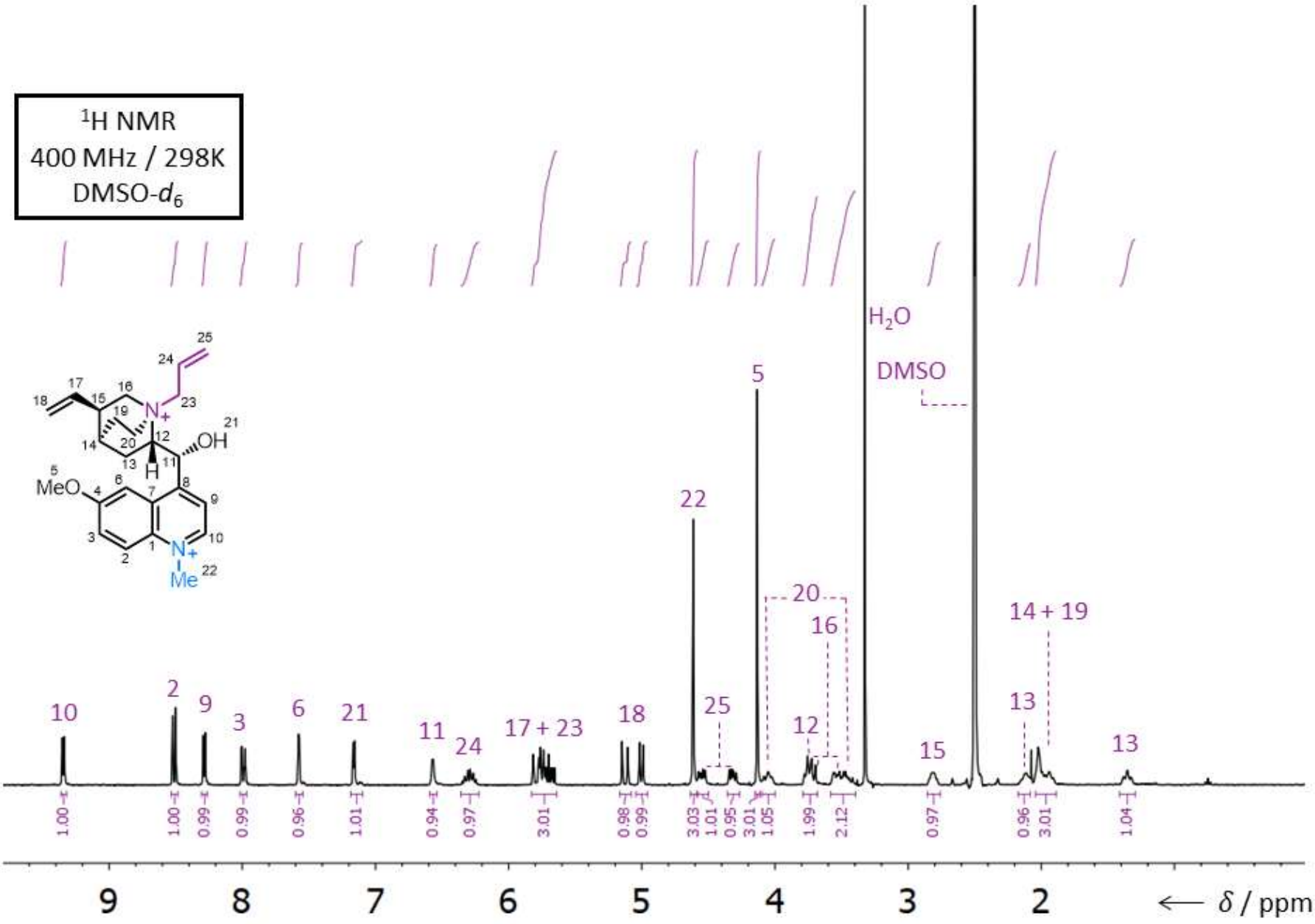

Fig. S7 ^{1}H NMR Spectrum of **1**·2Cl.

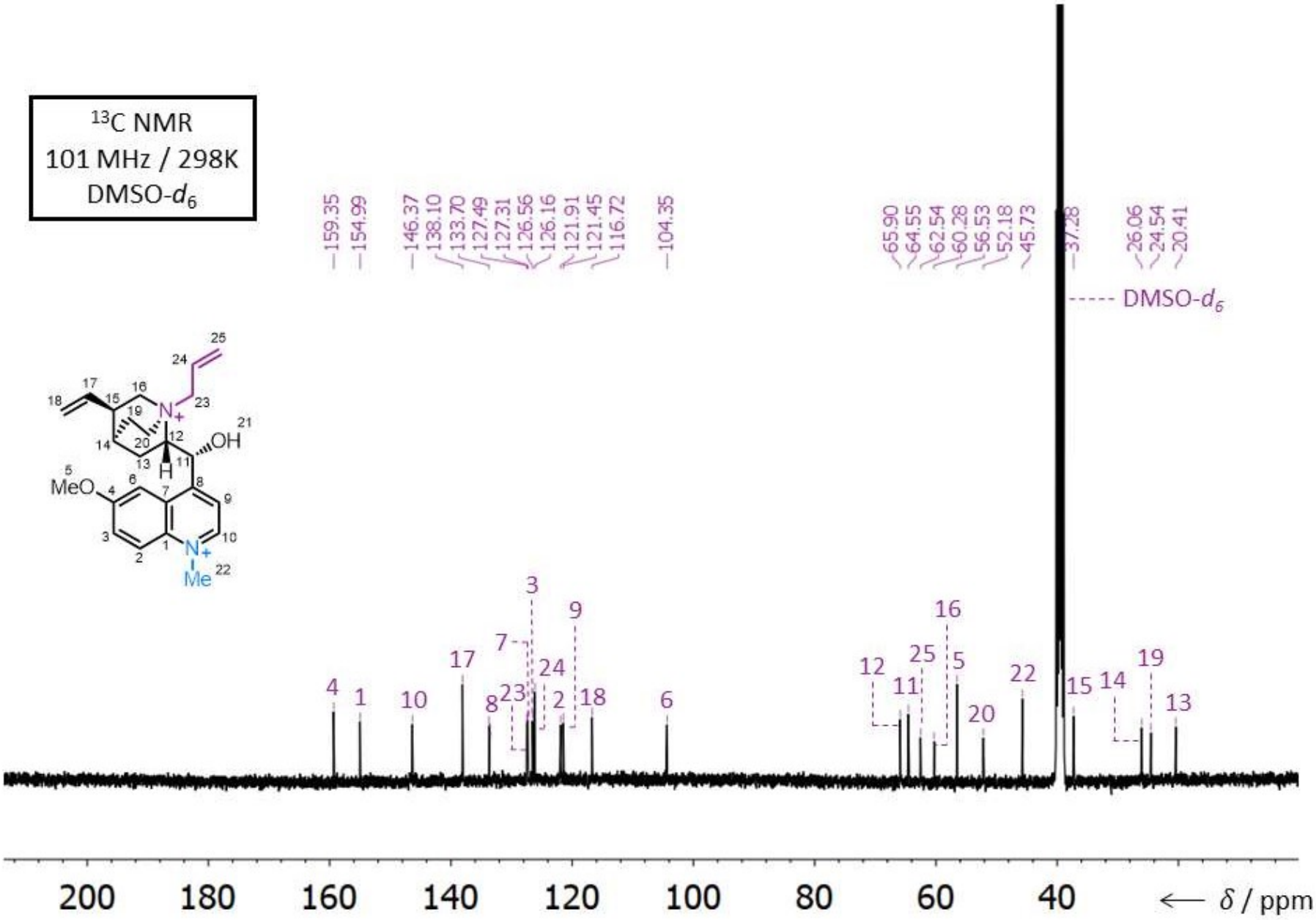

Fig. S8 ^{13}C NMR Spectrum of **1**·2Cl.

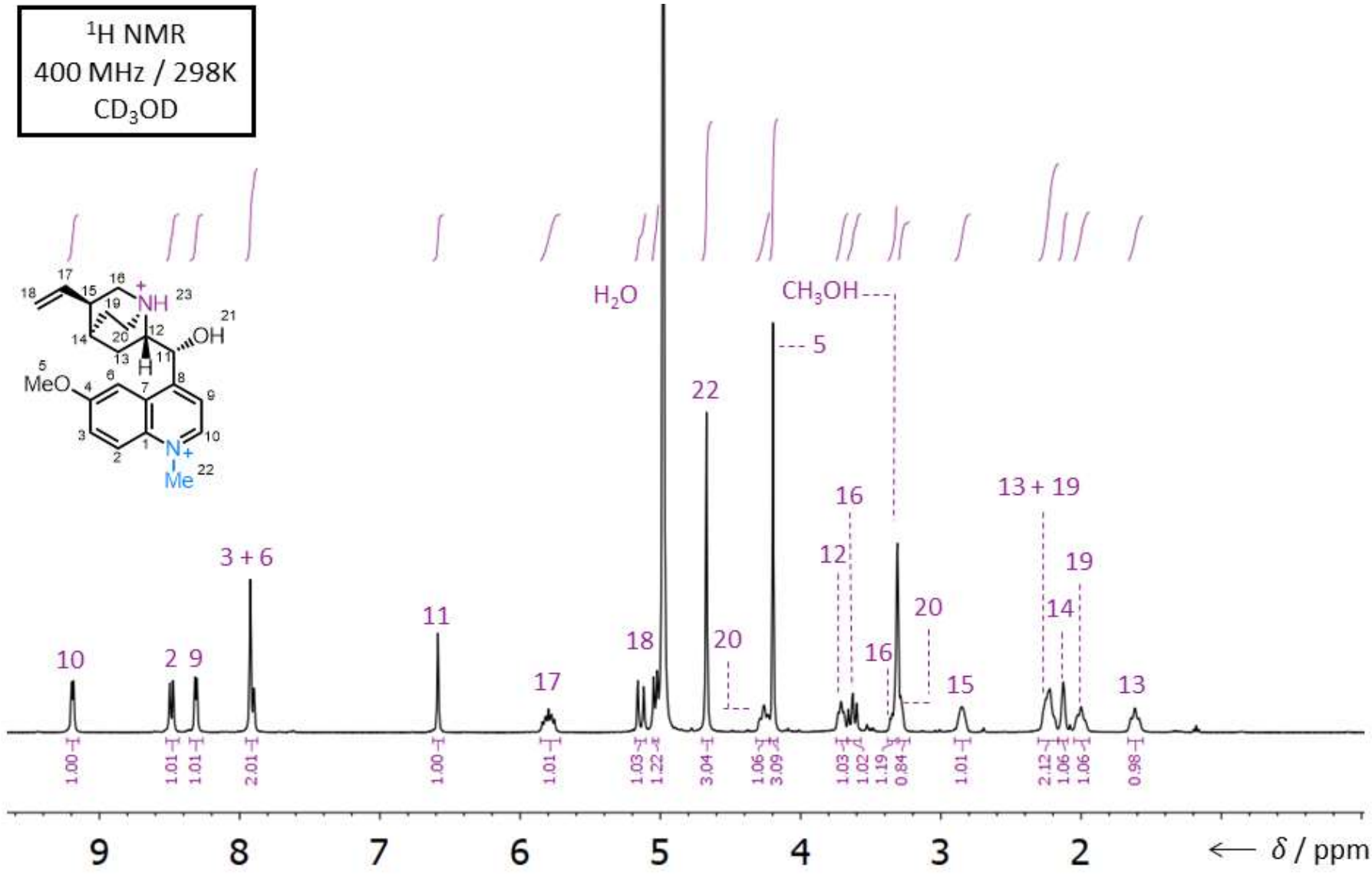

Fig. S9 [1]H NMR Spectrum of **H-iMeQn**·2Cl.

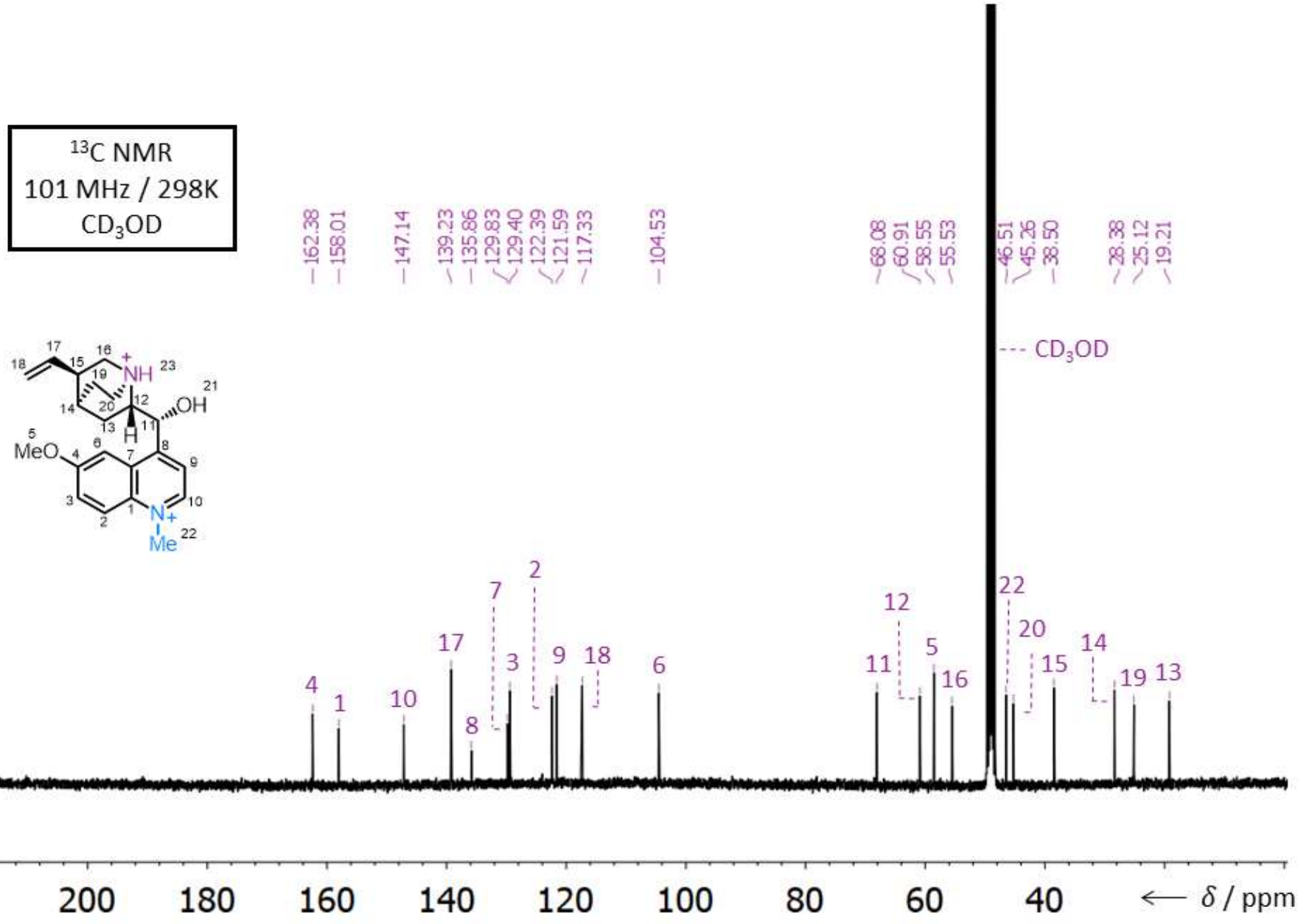

Fig. S10 ^{13}C NMR Spectrum of **H-iMeQn**·2Cl.

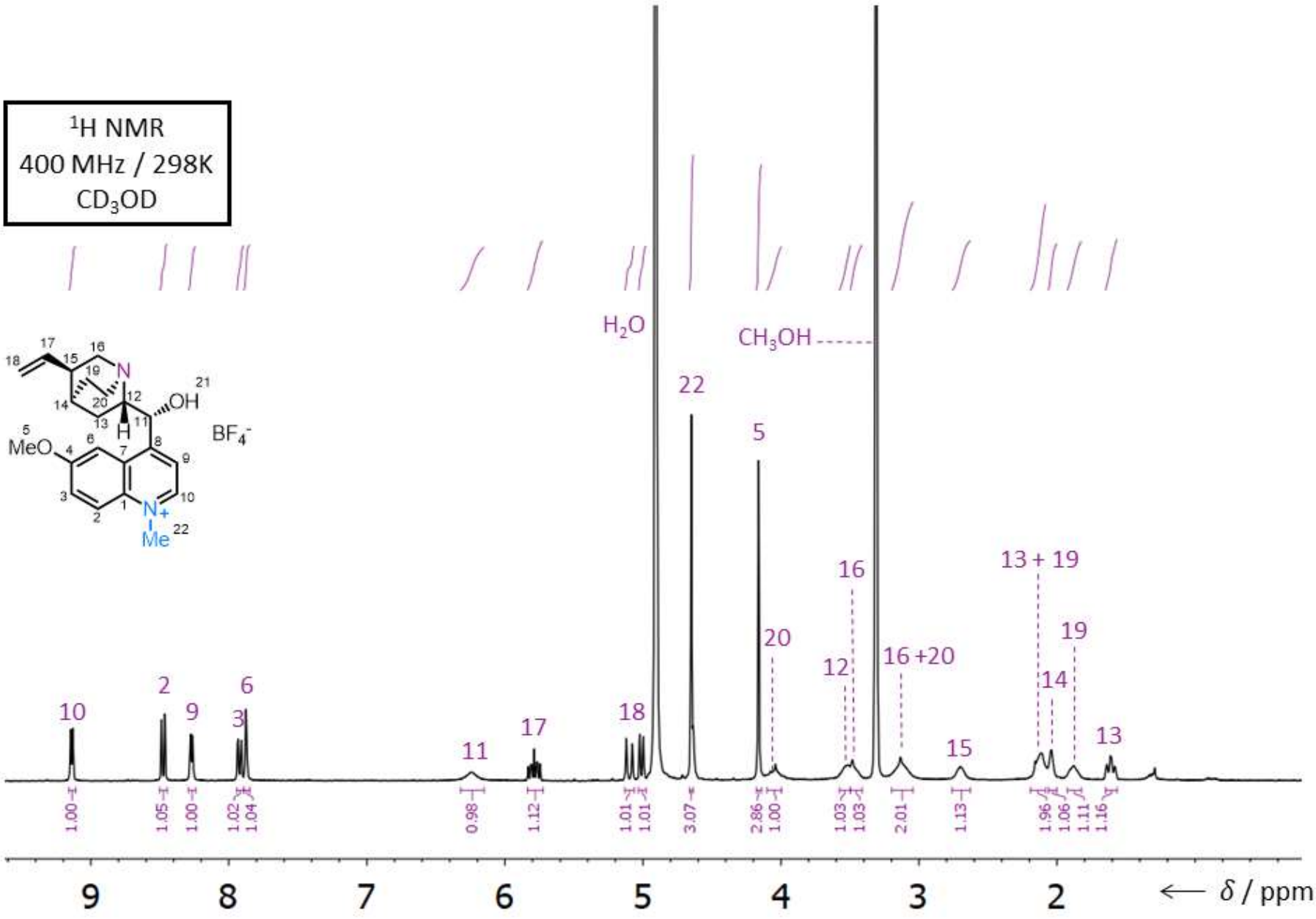

Fig. S11 ^{1}H NMR Spectrum of **iMeQn**·BF_4.

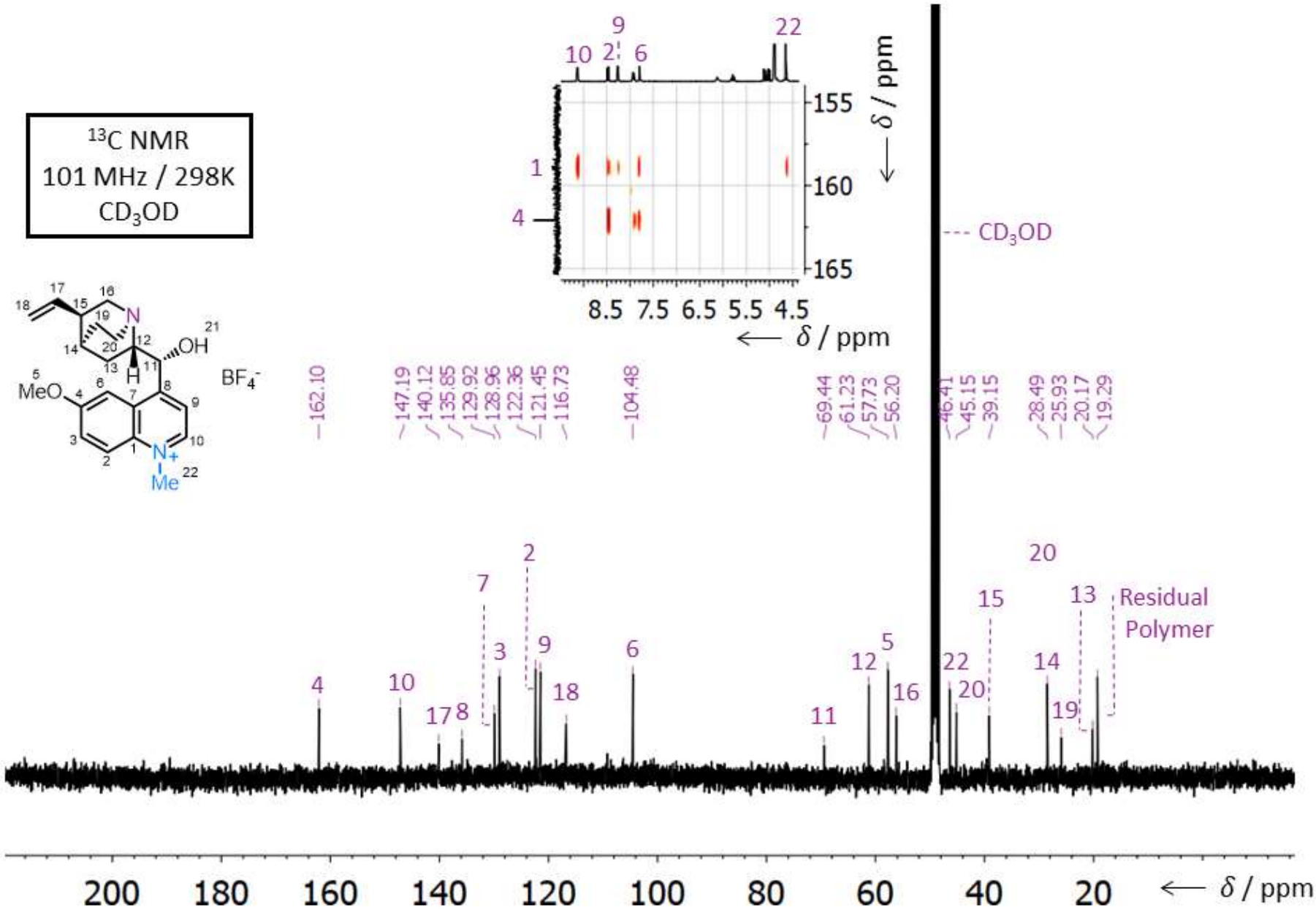

Fig. S12 ^{13}C NMR Spectrum of **iMeQn**·BF_4. Insert: Partial HMBC spectrum to show the ^{13}C resonance for C_1, which is not visible in the 1D spectrum.

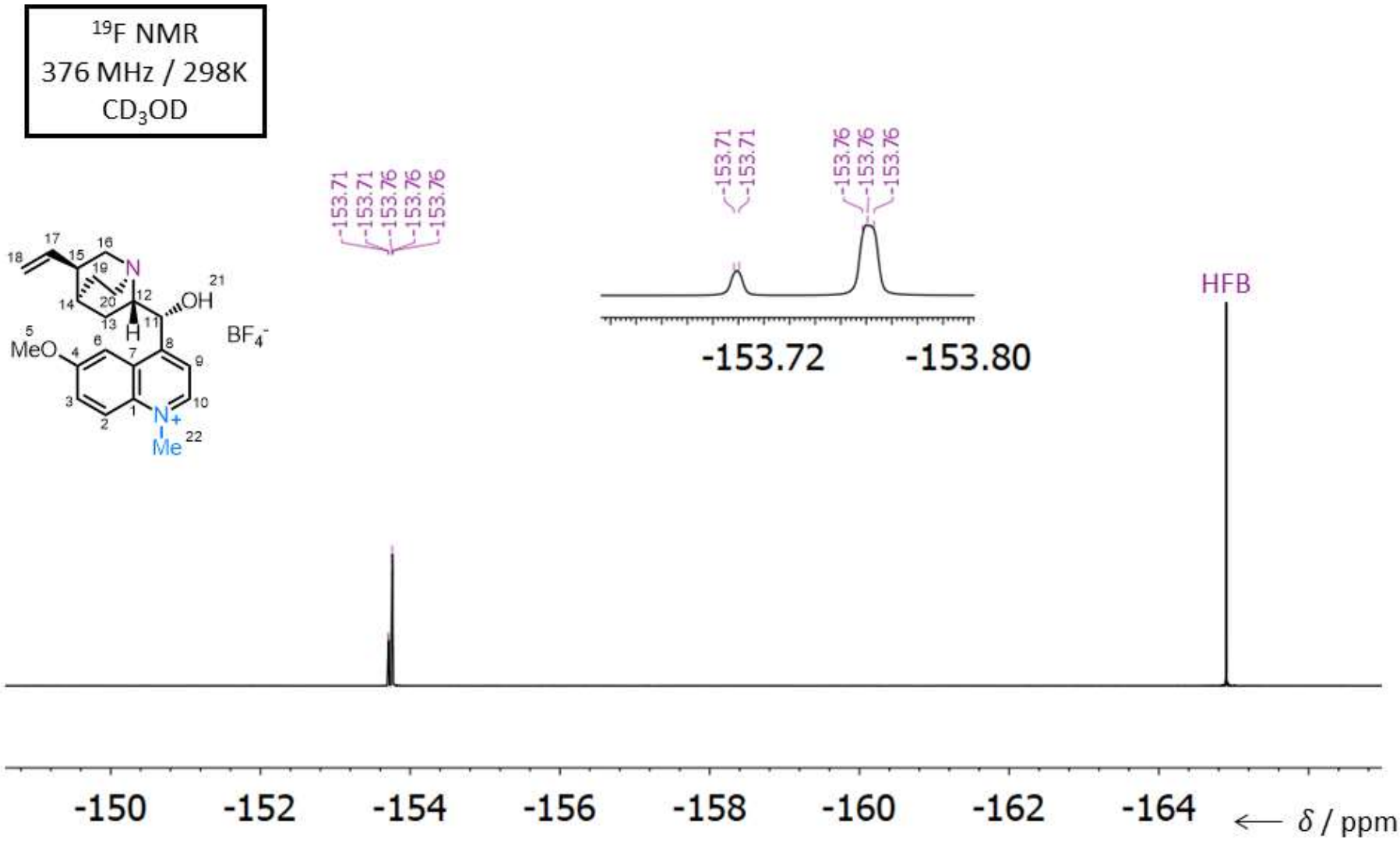

Fig. S13 ^{19}F NMR Spectrum of **iMeQn**·BF_4.

3.2. NMR Comparisons of Methylated and Protonated Quinines

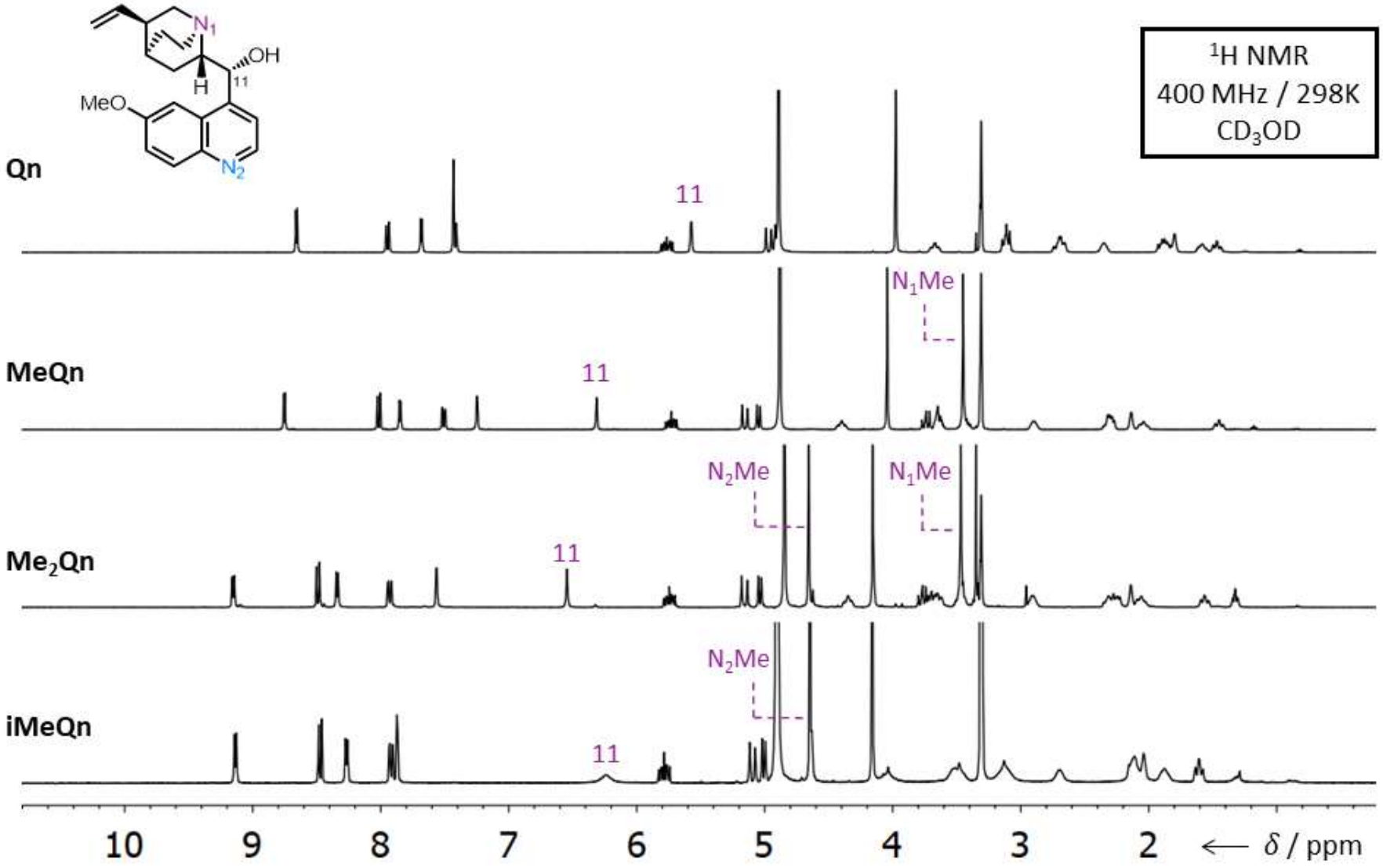

Fig. S14 Comparison of ^{1}H NMR spectra of **Qn**, **MeQn**·BF_4, **Me_2Qn**·$2BF_4$ and **iMeQn**·BF_4, demonstrating the deshielding of H_{11} upon alkylation and the characteristic Me resonances observed for the two N sites.

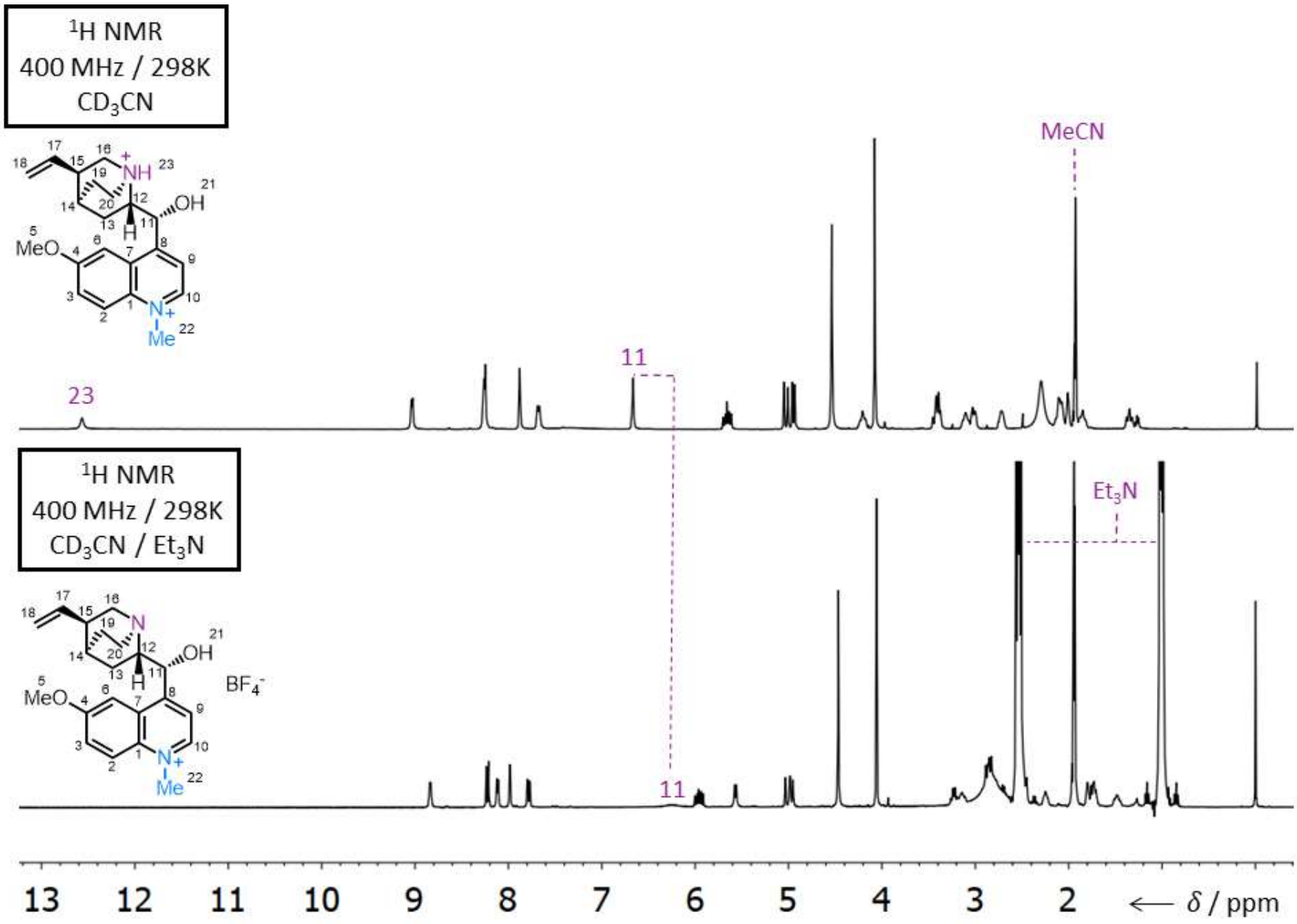

Fig. S15 Comparison of **H-iMeQn**·2BF_4 and **iMeQn**·BF_4 ^{1}H NMR spectra. The shift in the resonance of H_{11} is consistent with spectroscopic data in the literature for (de)protonation at N_1[8] and with the shifts observed (Figure S14) upon methylation.

4. X-Ray Crystallographic Analysis

4.1 **MeQn**·BF_4

Crystals of **MeQn**·BF_4 suitable for X-ray diffraction were grown by slow cooling of a saturated MeCN solution.

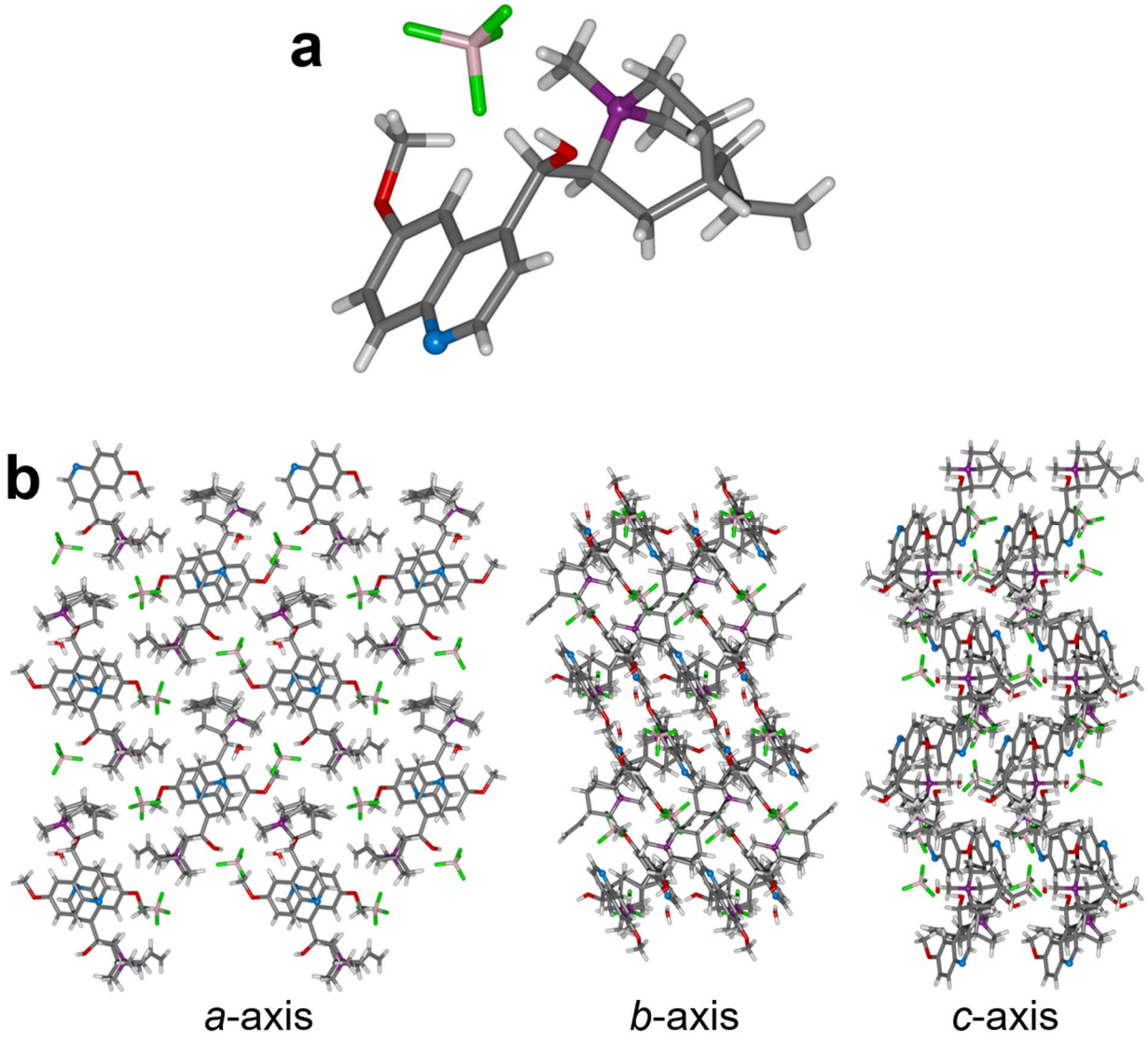

Fig. S16 (a) Solid-state structure and (b) crystal packing of **MeQn**·BF_4.

4.2 $Me_2Qn \cdot 2BF_4$

Crystals of **Me_2Qn**$\cdot 2BF_4$ suitable for X-ray diffraction were grown by slow cooling of a saturated MeCN solution.

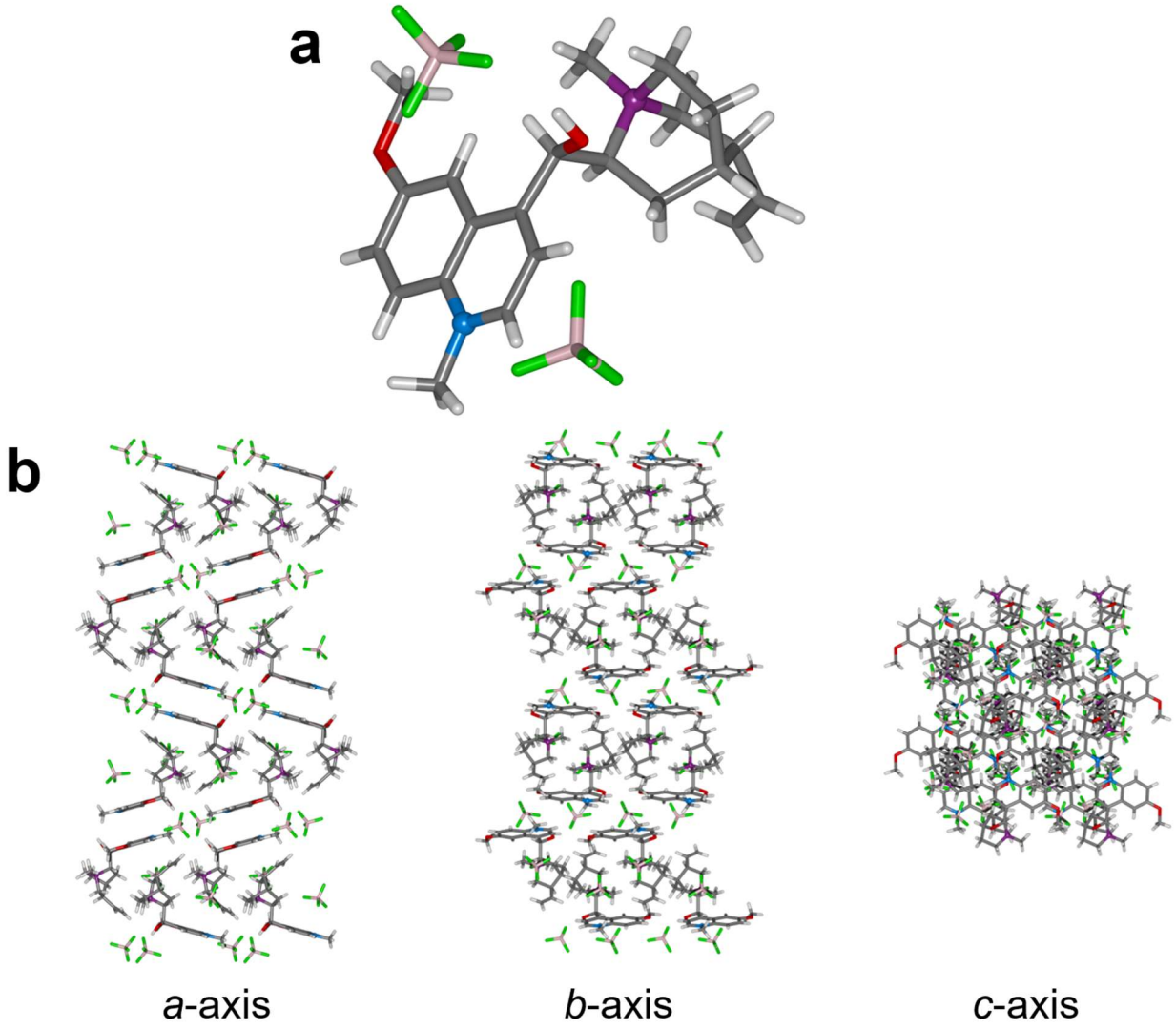

Fig. S17 (a) Solid-state structure and (b) crystal packing of **Me_2Qn**$\cdot 2BF_4$.

Table S1 Crystal Data and Refinement.

Compound	**MeQn**·BF_4	**Me_2Qn**·$2BF_4$
Empirical formula	$C_{21}H_{27}BF_4N_2O_2$ x 0.5 H_2O	$C_{22}H_{30}B_2F_8N_2O_2$
Formula weight	435.26	528.10
Temperature/K	120.0	120.0
Crystal system	monoclinic	orthorhombic
Space group	$P2_1$	$P2_12_12_1$
a/Å	8.0721(2)	9.6961(3)
b/Å	15.6353(5)	10.2407(3)
c/Å	16.4422(5)	23.6533(8)
α/°	90	90
β/°	98.2832(14)	90
γ/°	90	90
Volume/$Å^3$	2053.52(10)	2348.65(13)
Z	4	4
ρ_{calc} g/cm^3	1.408	1.494
μ/mm^{-1}	0.983	1.195
F(000)	916.0	1096.0
Crystal size/mm^3	0.42 × 0.26 × 0.09	0.39 × 0.28 × 0.12
2Θ range for data collection/°	5.432 to 139.976	7.474 to 144.936
Reflections collected	23769	27372
Independent refl., R_{int}	6963, 0.0308	4554, 0.0314
Data/restraints/parameters	6963/15/575	4554/0/445
Goodness-of-fit on F^2	1.068	1.067
Final R_1 indexes [I≥2σ (I)]	0.0424	0.0256
Final wR_2 indexes [all data]	0.1050	0.0651
Largest diff. peak/hole / e $Å^{-3}$	0.65/-0.59	0.31/-0.18
Flack parameter	0.01(6)	0.00(3)
Hooft parameter	0.05(4)	-0.01(3)

5. Photoluminescence Quantum Yield Measurements

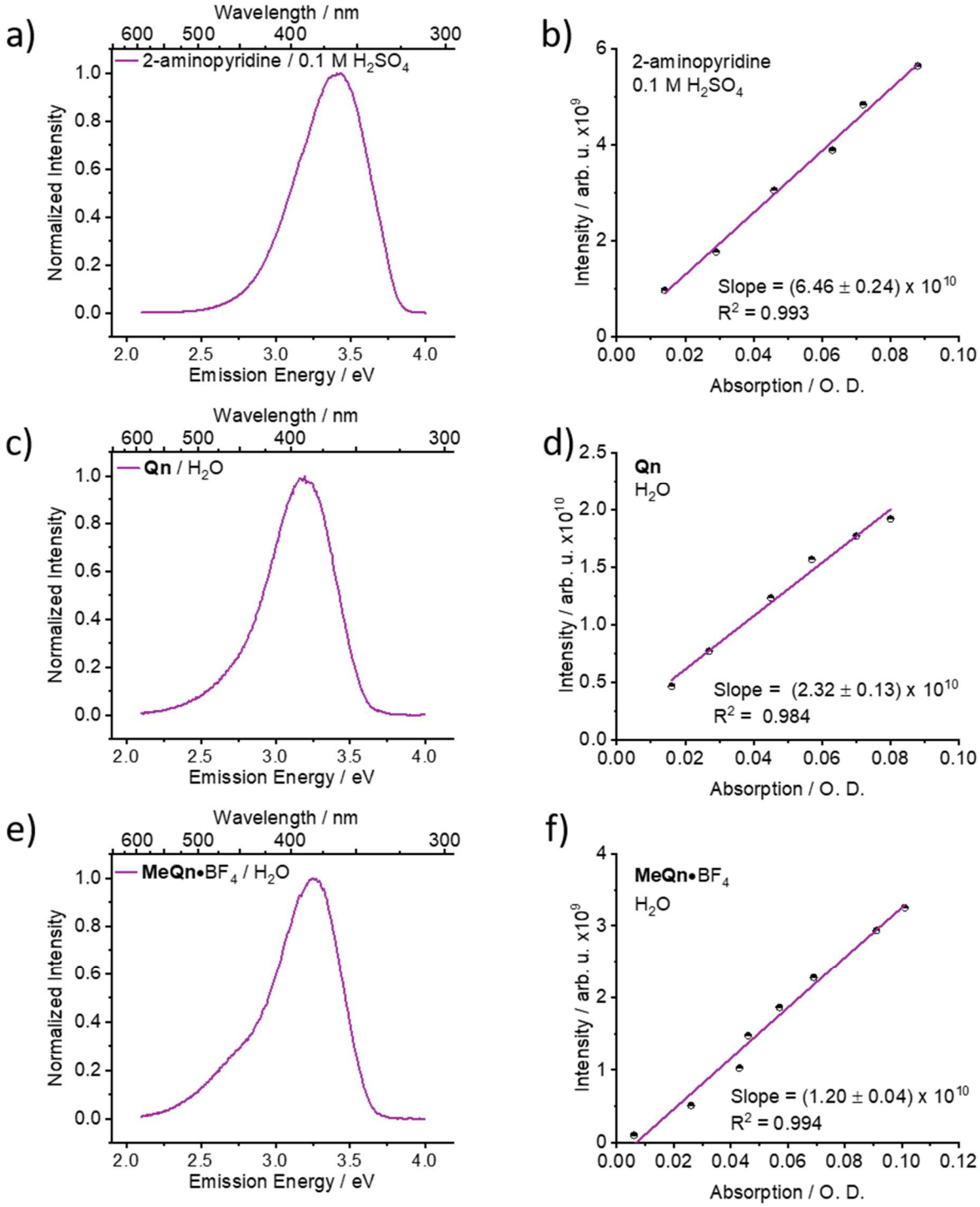

Fig. S18 The emission spectra and emission vs absorption slope of (a-b) 2-aminopyridine in 0.1 M $H_2SO_{4(aq)}$ as a standard, (c-d) **Qn** in H_2O and (e-f) **MeQn**·BF_4 in H_2O.

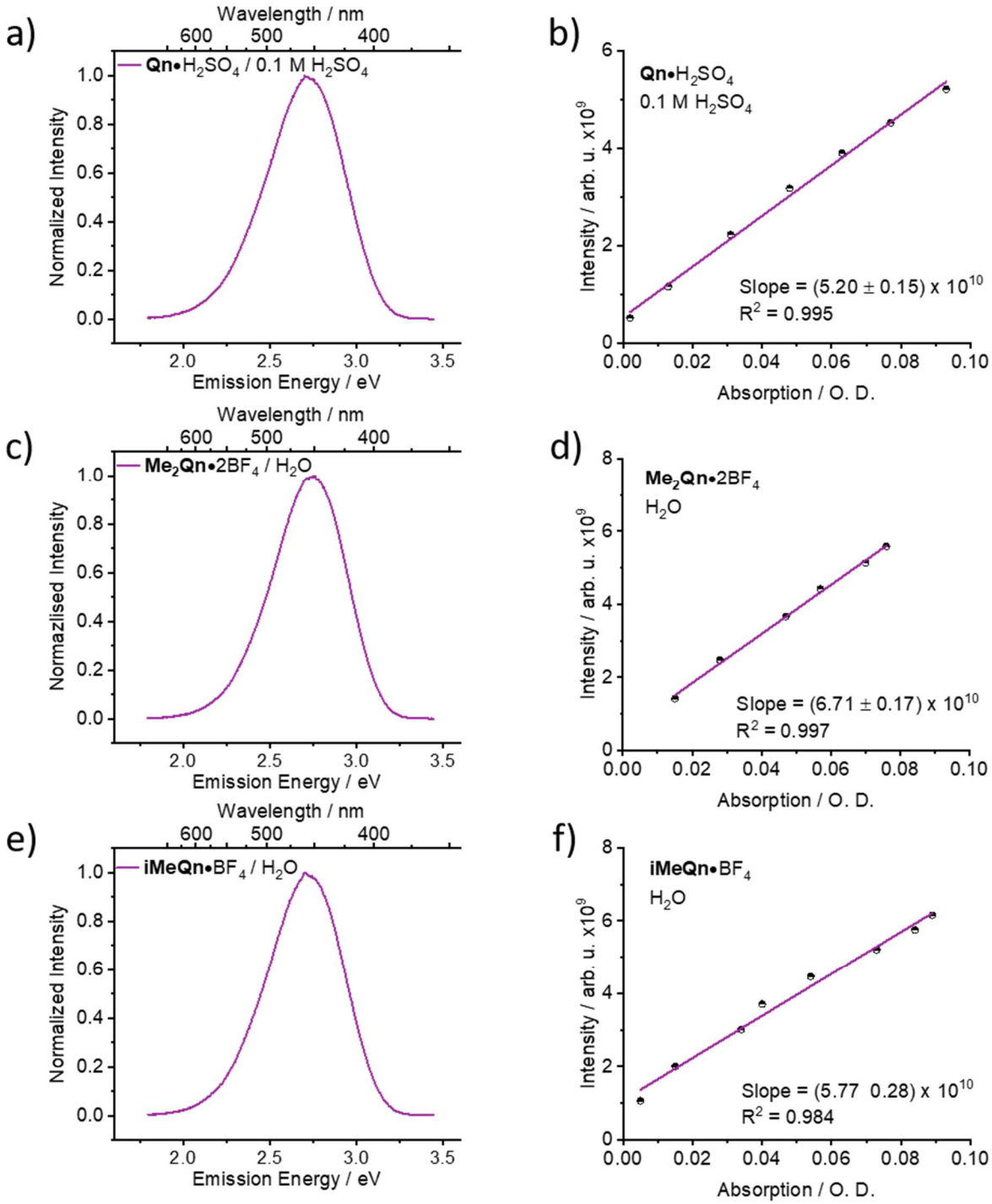

Fig. S19 The emission spectra and emission vs absorption slope of (a-b) **Qn**·H_2SO_4 in 0.1 M $H_2SO_{4(aq)}$ as a standard, (c-d) **Me_2Qn**·2BF_4 in H_2O and (e-f) **iMeQn**·BF_4 in H_2O.

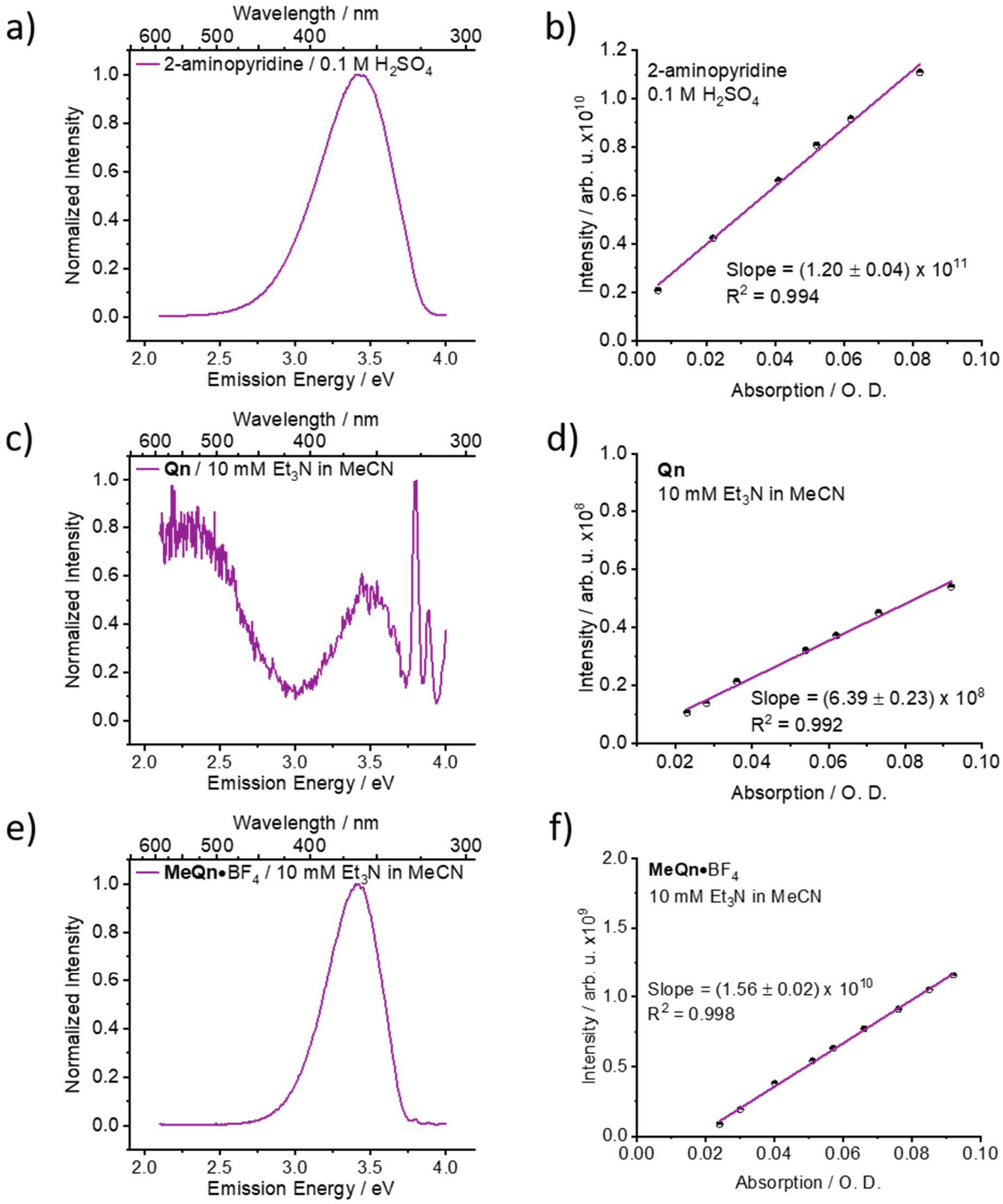

Fig. S20 The emission spectra and emission vs absorption slope of (a-b) 2-aminopyridine in 0.1 M $H_2SO_{4(aq)}$ as a standard, (c-d) **Qn** with 10 mM Et_3N in MeCN and (e-f) **MeQn**·BF_4 with 10 mM Et_3N in MeCN.

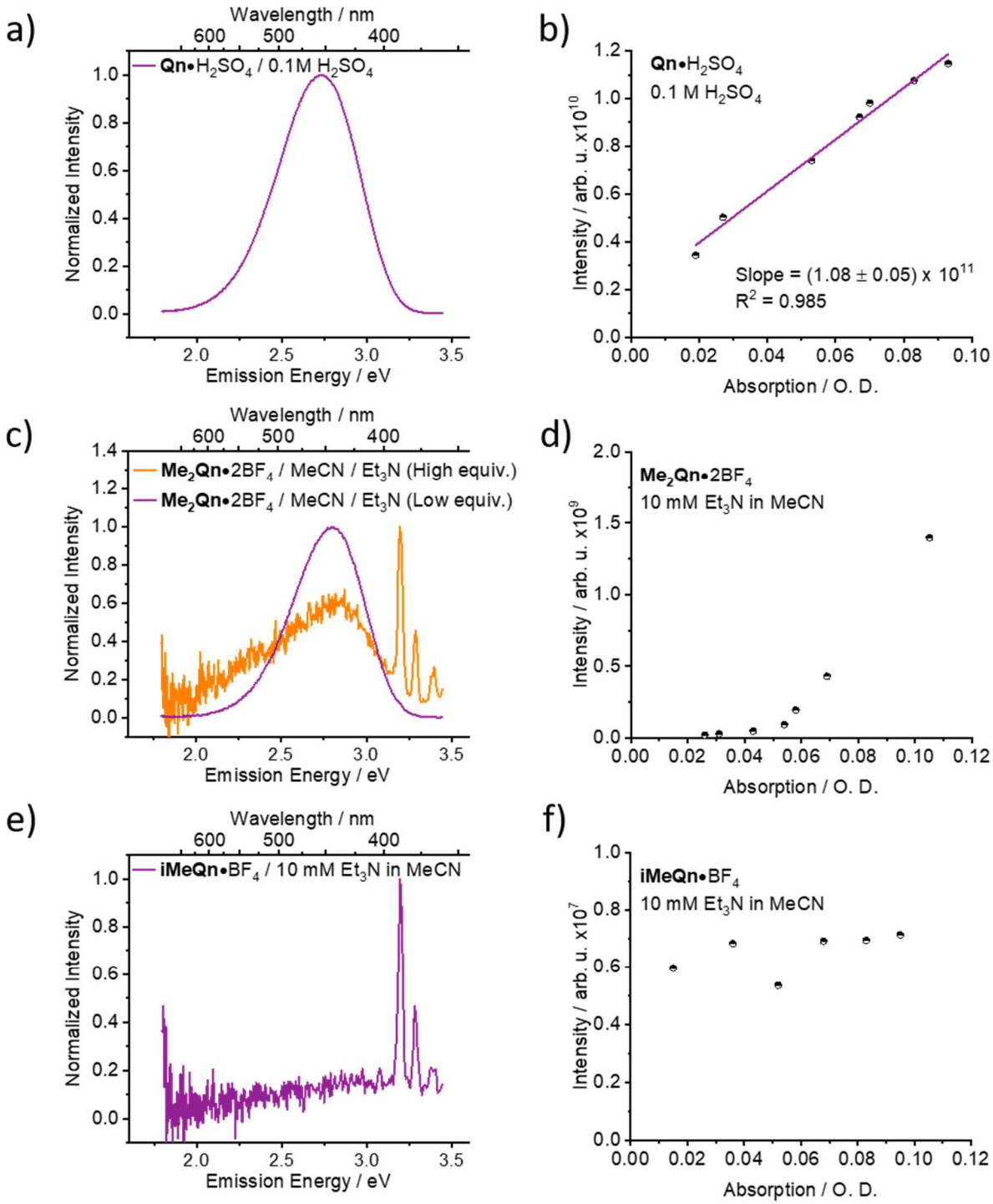

Fig. S21 The emission spectra and emission vs absorption slope of (a-b) **Qn**·H_2SO_4 in 0.1 M $H_2SO_{4(aq)}$ as a standard, (c-d) **Me₂Qn**·2BF_4 with 10 mM Et_3N in MeCN and (e-f) **iMeQn**·BF_4 with 10 mM Et_3N in MeCN.

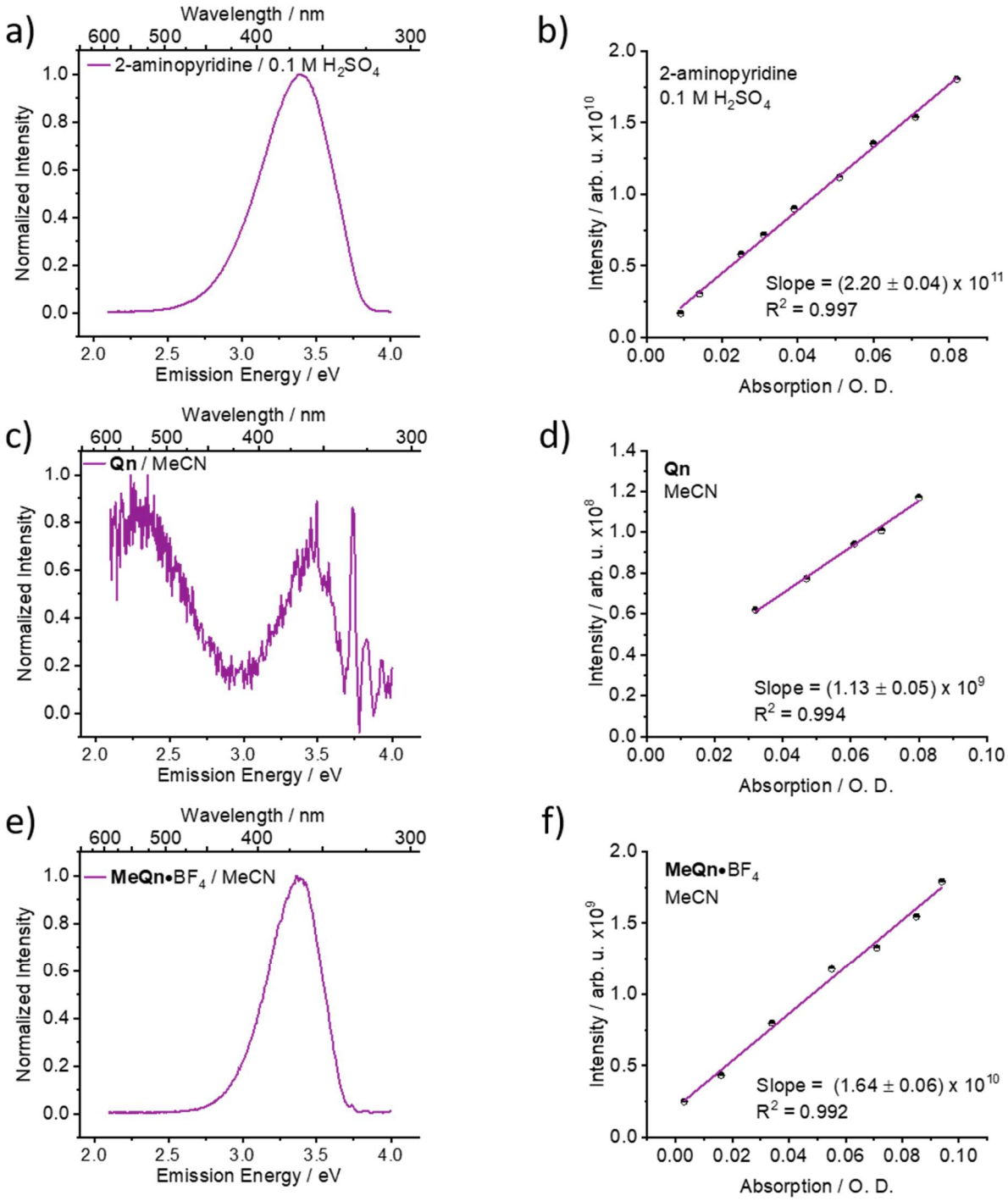

Fig. S22 The emission spectra and emission vs absorption slope of (a-b) 2-aminopyridine in 0.1 M $H_2SO_{4(aq)}$ as a standard, (c-d) **Qn** in MeCN and (e-f) **MeQn**·BF_4 in MeCN.

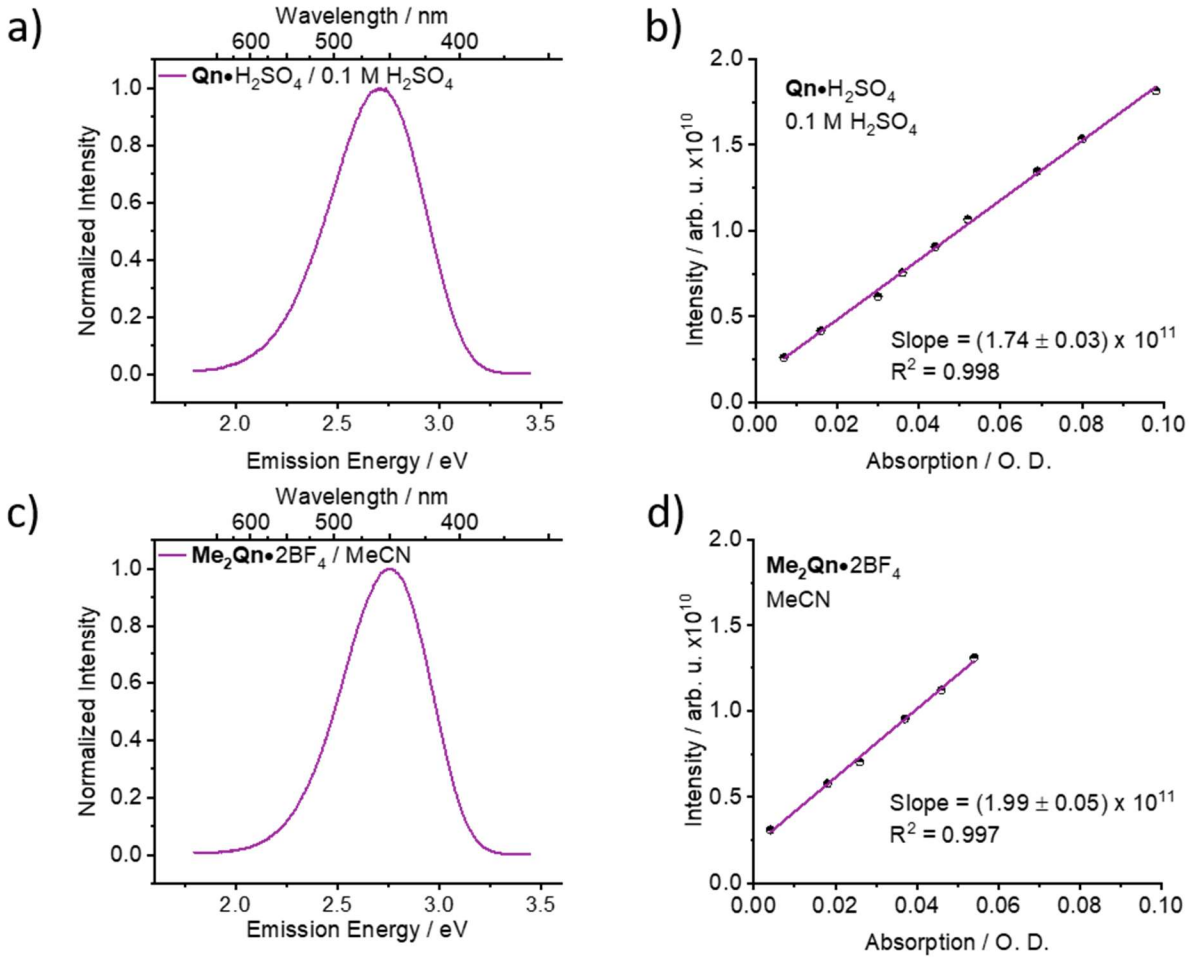

Fig. S23 The emission spectra and emission vs absorption slope of (a-b) **Qn**·H_2SO_4 in 0.1 M $H_2SO_{4(aq)}$ as a standard and (c-d) **Me_2Qn**·$2BF_4$ in MeCN.

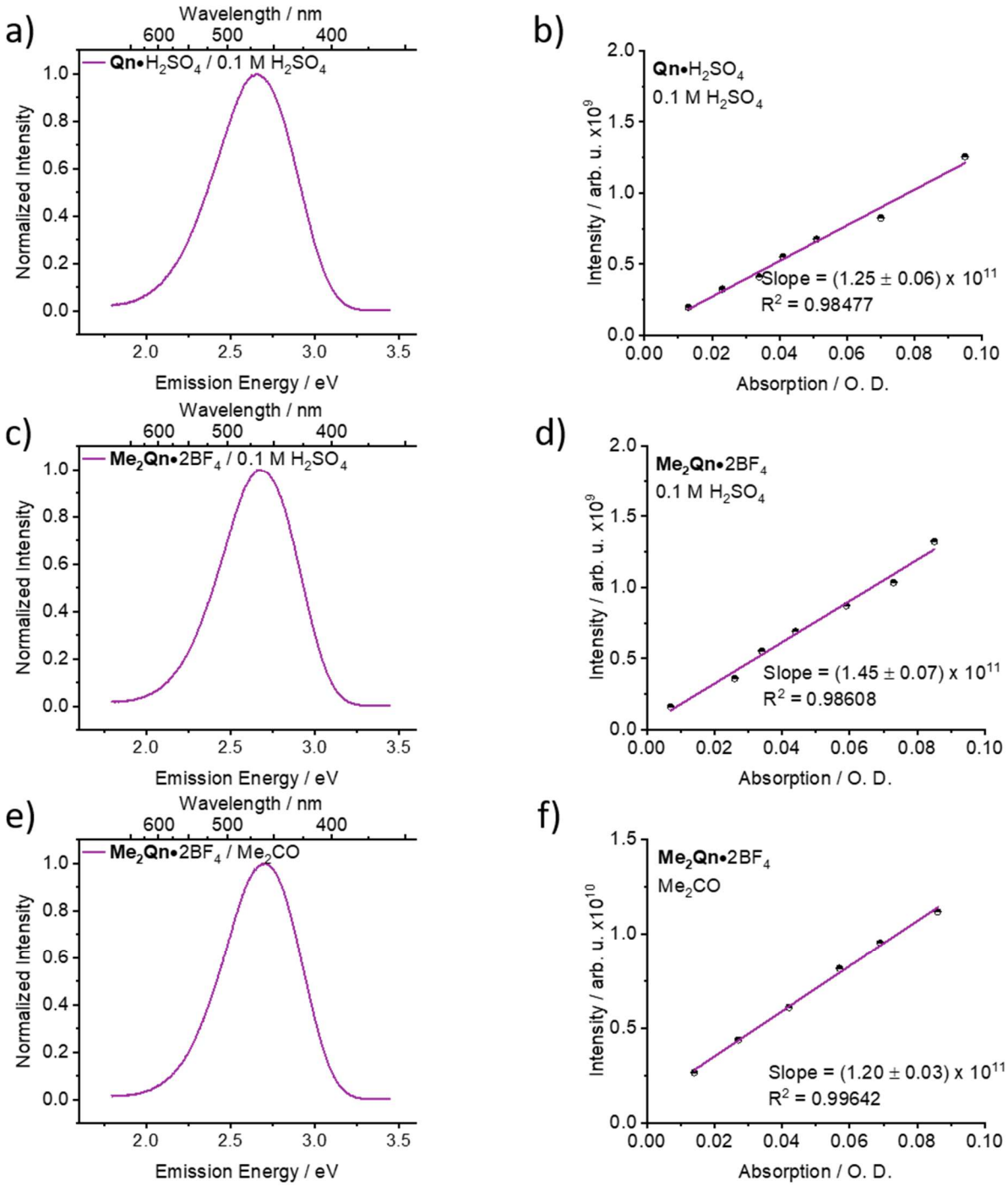

Fig. S24 The emission spectra and emission vs absorption slope of (a-b) **Qn**·H_2SO_4 in 0.1 M $H_2SO_{4(aq)}$ as a standard, (c-d) **Me₂Qn**·2BF_4 in 0.1 M H_2SO_4 and (e-f) **Me₂Qn**·2BF_4 in acetone (Me_2CO)

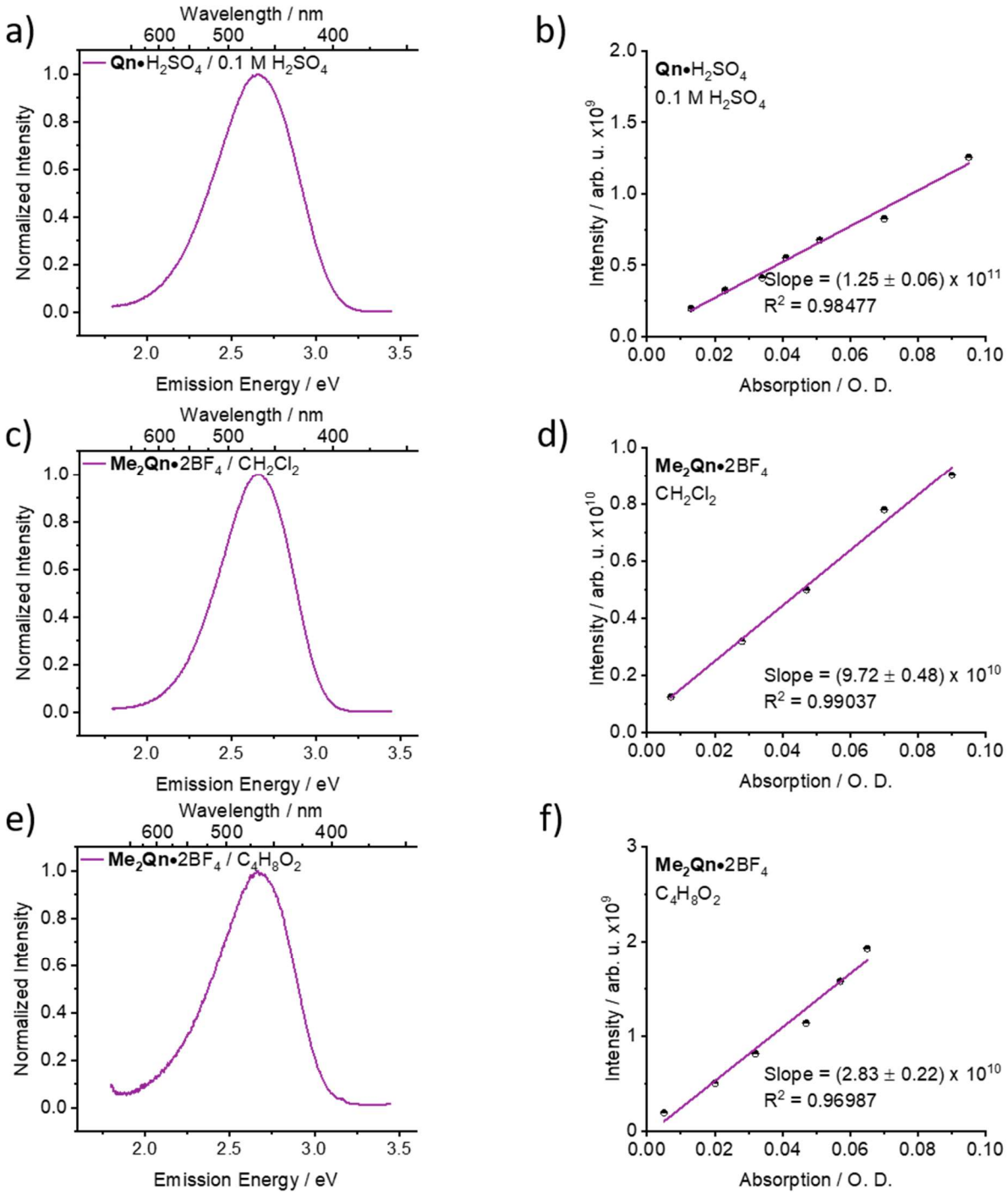

Fig. S25 The emission spectra and emission vs absorption slope of (a-b) **Qn**·H_2SO_4 in 0.1 M $H_2SO_{4(aq)}$ as a standard, (c-d) **Me₂Qn**·$2BF_4$ in dichloromethane (CH_2Cl_2) and (e-f) **Me₂Qn**·$2BF_4$ in ethyl acetate ($C_4H_8O_2$).

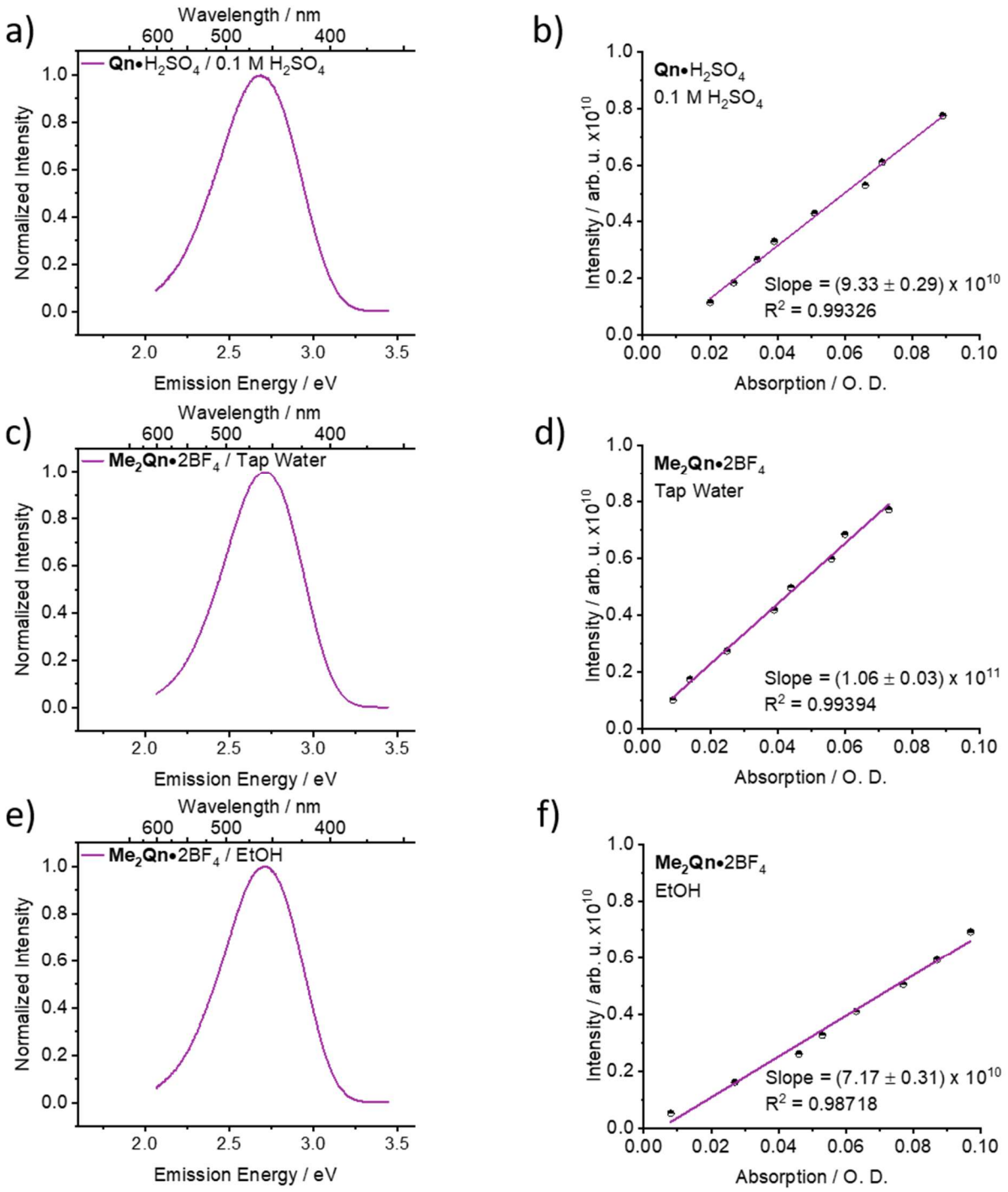

Fig. S26 The emission spectra and emission vs absorption slope of (a-b) **Qn**·H_2SO_4 in 0.1 M $H_2SO_{4(aq)}$ as a standard, (c-d) **Me₂Qn**·$2BF_4$ in tap water and (e-f) **Me₂Qn**·$2BF_4$ in ethanol (EtOH).

Table S2 PLQYs measured for **Me_2Qn**·$2BF_4$ in an extended series of solvents.

Solvent	Dielectric Constant, ε[9]	Polarity Index[10]	Φ / %
Deionised Water	88	1	70
Tap Water	-	-	62
0.1 M $H_2SO_{4(aq)}$	-	-	62
Acetonitrile (MeCN)	37.5	0.460	63
Ethanol (EtOH)	24.3	0.654	43
Acetone (Me_2CO)	20.7	0.355	54
Dichloromethane (CH_2Cl_2)	9.08	0.309	48
Ethyl Acetate (EtOAc)	6.4	0.228	13

6. Phosphorescence of Qn in a Zeonex Film

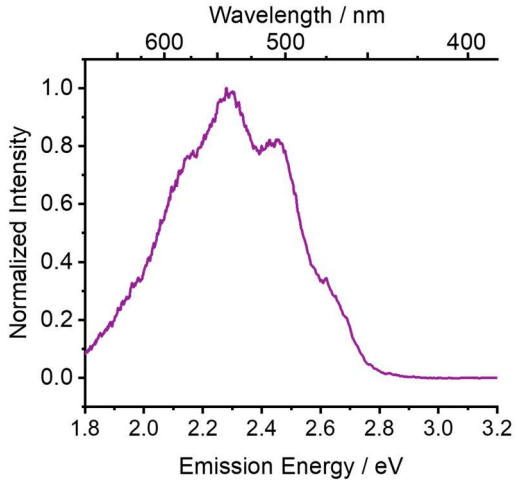

Fig. S27 The phosphorescence emission spectra of a 1 wt% film of **Qn** in zeonex. The film was prepared by dropcasting a PhMe solution and recorded at 40 ms delay and 80 K.

7. Theoretical study

Computational details

Ground-state geometry optimizations of **Qn** and its derivatives were performed both *in vacuo* and using an implicit acetonitrile solvent. We used a protonation of N1 and N2 instead of a methylation, but Table S7 below shows that the effect of such substitution is minimal for emission energies. We employed density functional theory (DFT) with the ωB97X-D exchange-correlation functional[11] and a 6-31G* basis set.[12] This functional contains both long-range and dispersion interaction corrections. Solvent effects were taken into account using self-consistent reaction field (SCRF) model, where the solvent is represented by a dielectric continuum. More specifically, we employed the integral equation formalism of the polarisable continuum model (IEFPCM).[13] Harmonic vibrational frequencies were computed to confirm the nature of all stationary points.

Excited electronic states were computed using linear-response time-dependent density functional theory (LR-TDDFT) at the ωB97X-D/6-31G* level of theory and systematically compared to results obtained with the wavefunction-based second-order algebraic diagrammatic construction method (ADC(2)),[14] used along with a cc-pVDZ basis set.[15] ADC(2) calculations were performed with frozen core and resolution of identity approximations. To justify the use of a small basis set, tests were conducted for comparison with the larger aug-cc-pVDZ basis set.[16]

Vertical transitions were calculated based on the optimized ground-state geometries using LR-TDDFT, with nonequilibrium linear-response IEFPCM solvation (acetonitrile). As our main focus is to determine the emission properties of the studied compounds, we also located minimum energy

structures on the potential energy surface of the first excited state (and also the second one for some specific cases). For these excited-state geometry optimizations, we used LR-TDDFT combined with equilibrium linear-response IEFPCM solvation (acetonitrile). Harmonic vibrational frequencies were computed for excited-state minima. The linear-response approach for implicit solvation models is known to provide reliable excited-state geometries, but less accurate emission energies.[17] Therefore, the emission energies were also computed with the state-specific approach as implemented in Gaussian09. ADC(2) excited-state optimizations were performed only in vacuo, and harmonic frequencies were not computed due to the high computational cost. To estimate the emission energy for the solvated systems, single-point ADC(2) computations with the conductor-like screening model (COSMO)[18] for solvation were performed *a posteriori* on the optimized gas phase geometries. This protocol relies on the assumption that the calculated excited-state structures are similar in gas and solvent phases. We also assume the equilibrium solvation limit, in which the electronic and nuclear degrees of freedom of the solvent adapt to the excited-state (rather than the ground-state) charge distribution of the solute.[19] It is important to note, however, that we do not attempt here to closely reproduce the experimental values with our calculations, but rather to detect the main qualitative changes in absorption and emission upon protonation of quinine.

Excited state characters were analysed by computing natural transition orbitals (NTO),[20] both with TDDFT and ADC(2). All DFT/LR-TDDFT calculations were performed with the Gaussian09 software,[21] while ADC(2) calculations were conducted with Turbomole 7.3.1 program package.[22] Molecular representations were produced with VMD 1.9.2.[23]

Supporting calculations

Quinine can have different conformations, and its stable conformers were analyzed in detail in earlier theoretical and experimental work.[24,25] Here, we have mainly focused our attention on the so called cis-γ-open(3) conformer, which was identified as the most stable conformer based on jet-cooled spectroscopy, vibrational circular dichroism and theoretical calculations.[25] The same conformer is found for the crystal structure of quinine.[26]

The absorption spectrum of quinine contains both locally excited (LE) bright ππ* transition localized on the quinoline moiety, and a higher-lying charge-transfer (CT) state in which the electron is transferred from a *n*(N) orbital of quinuclidine to a π* orbital of quinoline (*n*π*). As shown in Table S3, the LE(ππ*) state is the lowest excited singlet state both with ωB97X-D and ADC(2). At the ground-state (i.e. Franck-Condon) geometry, the CT(*n*π*) state lies higher in energy, and is likely to be overestimated by ωB97X-D. Using a larger basis set does not alter these trends – the relevant transitions are only slightly down shifted.

Table S3 Excited states of **Qn** (*in vacuo*) at the ground-state geometry optimized at ωB97X-D/6-31G* level. Excitation energies are given in eV, along with corresponding oscillator strengths (f).

	ωB97x-D/6-31G*	ωB97x-D/aug-cc-pVDZ	ADC(2)/cc-pVDZ	ADC(2)/aug-cc-pVDZ
S_1	4.47 (LE), f=0.0993	4.35 (LE), f=0.0992	4.27 (LE), f=0.0949	4.15 (LE), f=0.0979
S_2	4.72, f=0.0029	4.67, f=0.0019	4.63, f=0.0024	5.53, f=0.0018
S_3	4.92, f=0.0336	4.81, f=0.0296	4.89 (CT), f=0.0013	4.63 (CT), f=0.0010
S_4	5.44 (CT), f=0.0029	5.34 (CT), f=0.0020	4.97, f=0.0529	4.71, f=0.0061
S_5	5.79, f=0.0002	5.71, f=0.0029	5.51, f=0.0002	4.83, f=0.0400

Upon protonation of the N atoms having an available lone pair, the excited states are either shifted in energy or removed from the spectrum (as they cannot be formed anymore). Table S4 compares the absorption energies of the LE(ππ*) and CT(*n*π*) states of **Qn** and its protonated derivatives, **HQn**$^+$ (proton on N1), **iHQn**$^+$ (proton on N2) and **H$_2$Qn**$^{2+}$ (protons on N1 and N2) in acetonitrile solvent. Protonation of N1 prevents the formation of the CT(*n*π*) states, while protonation of N2 causes a large red-shift of the LE(ππ*) and CT(*n*π*) vertical transition (when latter exists). **H$_2$Qn**$^{2+}$ exhibits both effects.

Table S4 LE(ππ*) and CT(*n*π*) excited states of **Qn** and its protonated derivatives with ωB97X-D/6-31G* in acetonitrile solvent. Vertical transitions were evaluated at the ground-state geometries optimized at the same level of theory with DFT. Excitation energies are given in eV, along with corresponding oscillator strengths (f).

	Qn	**HQn**$^+$	**iHQn**$^+$	**H$_2$Qn**$^{2+}$
LE	4.43, f=0.1312	4.38, f=0.1402	3.93, f=0.1289	3.88, f=0.1263
CT	5.32, f=0.0025	-	4.06, f=0.0064	-

The calculated vertical emission energies (Table S5) indicate that protonation of N2 causes a significant red-shift of the emission as compared to the pristine **Qn**. However, the LE emission of **iHQn**$^+$ is expected to be quenched due to the presence of the CT state, i.e., the molecule is likely to undergo nonradiative decay. This is consistent with our experimental findings for the analogous methylated derivatives, which found barely detectable fluorescence for **iMeQn**$^+$. Interestingly, even in **Qn** the CT state falls down in energy upon geometry relaxation, and the nonradiative population exchange between LE and CT states becomes more likely (keeping in mind that CT energies are overestimated by ωB97X-D). Therefore, LE emission in **Qn** has very low intensity, while CT emission becomes almost equally pronounced (see Figure 1 in the main text). Protonation of N1 causes only

slight red-shift in emission. Again, **H_2Qn^{2+}** benefits from two effects; the colour of its fluorescence is altered, while deleterious nonradiative effects are less likely due to the lack of CT state.

Table S5 Vertical emission energies computed with ωB97X-D/6-31G* and ADC(2)/cc-pVDZ. Note that with ωB97X-D equilibrium linear-response solvation (acetonitrile) is used, while ADC(2) optimizations were performed in gas phase. Nevertheless, the qualitative conclusions are similar. Emission energies are given in eV, along with corresponding oscillator strengths (f).

		Qn	**HQn^+**	**$iHQn^+$**	**H_2Qn^{2+}**
ωB97X-D	LE	3.81 (S_1), f=0.2641	3.76 (S_1), f=0.2635	converge to CT	3.21 (S_1), f=0.1741
	CT	3.20 (S_1), f=0.0291	-	2.20 (S_1), f=0.0074	-
ADC(2)	LE	3.75 (S_1), f=0.1078	3.59 (S_1), f=0.1262	2.69 (S_2; above CT), f=0.0777	2.58 (S_1), f=0.0924
	CT	2.44 (S_1), f=0.0071	-	1.01 (S_1), f=0.0019	-

We have also evaluated emission energies based on a state-specific solvation schemes (Table S6), in which solvent is supposed to fully equilibrate with the excited state from the solute, while the ground state of the solute is treated in a non-equilibrium limit. The underlying assumption is that the excited-state lifetime is sufficiently long such that the slow and fast degrees of freedom of the solvent have sufficient time to adapt.[19] One possible explanation for the too low emission energies of the CT states could be related to a breakdown of this assumption, the CT states being too short lived to allow for a full relaxation of the solvent (leading to an overestimation of relaxation effects in the calculations). This effect is particularly striking for **Qn**, which exhibits experimentally an emission band centred at around 2.2 eV, see Figure 1). We note here that such underestimation of charge transfer bands with state-specific implicit solvent models were reported in the literature.[27,28] Explicit solvent effects might be required to improve the description of this band. The LE states of **Qn** and **$iHQn^+$** may also not have sufficiently long lifetime due to the nonradiative effects mentioned above, but the variations in LE emission energy with and without state-specific solvation are generally not very large.

Table S6 Emission energies from state-specific equilibrium solvation (acetonitrile). The optimised geometries are the same as those in Table S5, but additional single-point computations were conducted. Emission energies are given in eV.

		Qn	HQn^+	$iHQn^+$	H_2Qn^{2+}
ωB97x-D	LE	3.75	3.69	-	3.00
	CT	1.41	-	1.01	-
ADC(2)	LE	3.61	3.47	2.56	2.43
	CT	1.46	-	0.36	-

Finally, Table S7 shows that methylation has almost the same impact on the calculated fluorescence as protonation.

Table S7 Comparison of vertical emission energies for the protonated and methylated **Qn** derivatives. Excited states were optimised with ωB97X-D/6-31G* and equilibrium linear-response solvation (acetonitrile). Emission energies are given in eV, along with corresponding oscillator strengths (f).

	HQn^+	$iHQn^+$	H_2Qn^{2+}
LE	3.76 (S_1), f=0.2635	converge to CT	3.21 (S_1), f=0.1741
CT	-	2.20 (S_1), f=0.0074	-
	$MeQn^+$	$iMeQn^+$	Me_2Qn^{2+}
LE	3.75 (S_1), f=0.2574	converge to CT	3.23 (S_1), f=0.1840
CT	-	2.23 (S_1), f=0.0088	-

7. References

1 A. T. R. Williams, S. A. Winfield and J. N. Miller, *Analyst*, 1983, **108**, 1067.

2 W. H. Melhuish, *J. Phys. Chem.*, 1961, **65**, 229–235.

3 R. Rusakowicz and A. C. Testa, *J. Phys. Chem.*, 1968, **72**, 2680–2681.

4 O. V. Dolomanov, L. J. Bourhis, R. J. Gildea, J. A. K. Howard and H. Puschmann, *J. Appl. Crystallogr.*, 2009, **42**, 339–341.

5 G. M. Sheldrick, *Acta Crystallogr. Sect. A Found. Crystallogr.*, 2008, **64**, 112–122.

6 H. D. Flack, *Acta Crystallogr. Sect. A Found. Crystallogr.*, 1983, **39**, 876–881.

7 R. W. W. Hooft, L. H. Straver and A. L. Spek, *J. Appl. Crystallogr.*, 2008, **41**, 96–103.

8 M. Kubicki, T. Borowiak, K. Gawrońska and J. Gawroński, *Zeitschrift fur Naturforsch. - Sect. B J. Chem. Sci.*, 2000, **55**, 1083–1088.

9 Dixon Valve Dielectric Constants, https://www.dixonvalve.com/sites/default/files/product/files/brochures-literature/dielectric-constant-values.pdf, (accessed 24 February 2020).

10 C. Reichardt, *Solvents and Solvent Effects in Organic Chemistry*, Wiley, 2002.

11 J.-D. Chai and M. Head-Gordon, *Phys. Chem. Chem. Phys.*, 2008, **10**, 6615.

12 R. Krishnan, J. S. Binkley, R. Seeger and J. A. Pople, *J. Chem. Phys.*, 1980, **72**, 650–654.

13 J. Tomasi, B. Mennucci and R. Cammi, *Chem. Rev.*, 2005, **105**, 2999–3093.

14 A. Dreuw and M. Wormit, *Wiley Interdiscip. Rev. Comput. Mol. Sci.*, 2015, **5**, 82–95.

15 T. H. Dunning, *J. Chem. Phys.*, 1989, **90**, 1007–1023.

16 R. A. Kendall, T. H. Dunning and R. J. Harrison, *J. Chem. Phys.*, 1992, **96**, 6796–6806.

17 R. Improta, G. Scalmani, M. J. Frisch and V. Barone, *J. Chem. Phys.*, 2007, **127**, 074504.

18 A. Klamt and G. Schüürmann, *J. Chem. Soc. Perkin Trans. 2*, 1993, 799–805.

19 B. Lunkenheimer and A. Köhn, *J. Chem. Theory Comput.*, 2013, **9**, 977–994.

20 R. L. Martin, *J. Chem. Phys.*, 2003, **118**, 4775–4777.

21 M. J. Frisch, G. W. Trucks, H. B. Schlegel, G. E. Scuseria, M. A. Robb, J. R. Cheeseman, G. Scalmani, V. Barone, G. A. Petersson, H. Nakatsuji, X. Li, M. Caricato, A. Marenich, J. Bloino, B. G. Janesko, R. Gomperts, B. Mennucci, H. P. Hratchian, J. V. Ortiz, A. F. Izmaylov, J. L. Sonnenberg, D. Williams-Young, F. Ding, F. Lipparini, F. Egidi, J. Goings, B. Peng, A. Petrone, T. Henderson, D. Ranasinghe, V. G. Zakrzewski, J. Gao, N. Rega, G. Zheng, W. Liang, M. Hada, M. Ehara, K. Toyota, R. Fukuda, J. Hasegawa, M. Ishida, T. Nakajima, Y. Honda, O. Kitao, H. Nakai, T. Vreven, K. Throssell, J. A. Montgomery Jr, J. E. Peralta, F. Ogliaro, M. Bearpark, J. J. Heyd, E. Brothers, K. N. Kudin, V. N. Staroverov, T. Keith, R. Kobayashi, J. Normand, K. Raghavachari, A. Rendell, J. C. Burant, S. S. Iyengar, J. Tomasi, M. Cossi, J. M. Millam, M. Klene, C. Adamo, R. Cammi, J. W. Ochterski, R. L. Martin, K. Morokuma, O. Farkas, J. B. Foresman and D. J. Fox, *Gaussian, Inc., Wallingford CT*, 2016.

22 F. Furche, R. Ahlrichs, C. Hättig, W. Klopper, M. Sierka and F. Weigend, *Wiley Interdiscip. Rev. Comput. Mol. Sci.*, 2014, **4**, 91–100.

23 W. Humphrey, A. Dalke and K. Schulten, *J. Mol. Graph.*, 1996, **14**, 33–38.

24 M. K. Bilonda, L. Mammino and S. Scheiner, *Molecules*, 2017, **22**, 1–13.

25 A. Sen, A. Bouchet, V. Lepère, K. Le Barbu-Debus, D. Scuderi, F. Piuzzi and A. Zehnacker-Rentien, *J. Phys. Chem. A*, 2012, **116**, 8334–8344.

26 B. Pniewska and A. Suszko-Purzycka, *Acta Crystallogr. Sect. C Cryst. Struct. Commun.*, 1989, **45**, 638–642.

27 P. Kautny, F. Glöcklhofer, T. Kader, J. M. Mewes, B. Stöger, J. Fröhlich, D. Lumpi and F. Plasser, *Phys. Chem. Chem. Phys.*, 2017, **19**, 18055–18067.

28 J. M. Mewes, J. M. Herbert and A. Dreuw, *Phys. Chem. Chem. Phys.*, 2017, **19**, 1644–1654.